Classical-quantum crossovers in quasi-one-dimensional electron-hole systems: Exciton-Mott physics and interband optical spectra

Takuya Yoshioka and Kenichi Asano
Department of Physics, Osaka University, Toyonaka, Osaka, 560-0043, Japan
(Received 2 June 2012; published 10 September 2012)

We study quasi-one-dimensional electron-hole (e-h) systems by applying a self-consistent screened T-matrix approximation (SSTA), which can treat an e-h pair embedded in the background of the exciton-plasma mixture, characterized by the exciton ionization ratio. Two classical-quantum crossovers are found. The first crossover takes place as the drastic suppression of ionization ratio, representing the onset of the quantum dissociation of the exciton (binding-energy reduction and level-broadening effects). The second one can be seen in a gradual change in the interband absorption-gain and photoluminescence spectra: Moss-Burstein effects become significant, and the e-h plasma starts to dominate the optical gain. Most of the features of the absorption-gain spectra observed in the recent experiments can be captured semiquantitatively by our SSTA.

DOI: 10.1103/PhysRevB.86.115314 PACS number(s): 71.35.Lk, 71.35.Ee, 78.67.Lt

I. INTRODUCTION

Systems consisting of the same number of electrons and holes provide stages for the fundamental research on the many-body effects in the condensed matter. In fact, they exhibit numbers of characteristic phases induced by the intercarrier Coulomb interaction under the thermal equilibrium; an insulating exciton-gas phase at low electron-hole (e-h) density and low temperature, and a metallic e-h plasma phase at high e-h density or high temperature. Between them, there exists an exciton-Mott crossover[1–10] or transition.[1,3,9–19] Even a quantum condensation (e-h pairing) is predicted theoretically in the ultracold e-h systems, namely, the Bose-Einstein condensation of excitons[20–23] and the Bardeen-Cooper-Schrieffer state of e-h Cooper pairs,[24,25] which are connected via a crossover.[26–30] The uniqueness of the e-h system is the long-range nature of interaction, and the keen competition between the repulsive and the attractive interactions. This makes sharp contrast with the lattice systems with repulsive short-range interaction, e.g., Hubbard models, in which the many-body effects have been also intensively studied.

Thermalized e-h systems are actually realized in the nondoped semiconductors under a strong photoexcitation because the intraband relaxation is usually much faster than the interband one. They can also be found in the various semimetals, such as divalent metals, type-II semiconductor structures, and so on.[1,31] The exciton-Mott crossover is particularly important in the application to the laser devices since the population inversion in e-h plasma is a source of the optical gain. In the absence of many-body effects, it is obvious that the device performances are improved by using low-dimensional structures, e.g., quantum wells (two dimension), and quantum wires (one dimension). Since low dimensionality enhances the density of states in the vicinity of the band edge, a lower threshold, a higher differential gain, and a narrower bandwidth are expected there.[32–35] However, such advantages may be hindered by the many-body effects; the excitonic effects are enhanced by the spatial confinement in low-dimensional systems,[36–38] which might prevent the formation of e-h plasma. Further, the intercarrier scattering rates near the Fermi level might be quite large in quasi-one-dimensional (quasi-1D) systems even at low temperature.[39] This non-Fermi-liquid nature implies a large broadening of optical spectra, which can be a disadvantage of the optical gain. Strong excitonic effects also demand the reconsideration on the screening effects, i.e., once e-h pairs form charge neutral excitonic bound states, they no longer give relevant contribution to the screening effects.

The quality of the quasi-1D e-h systems has been much improved since the early observation of lasing[40–48] and photoluminescence (PL) spectra.[49–53] They can now provide rich experimental outcomes to test the above issue. In recent PL measurements on the T-shape quantum wires,[54–57] a new peak is found in the lower-energy side of the excitonic peak. The energies of both new and excitonic peaks are almost unshifted, and the intensity is transferred from the latter to the former, as the e-h density is increased. As for the absorption-gain spectra,[54] the sharp exciton absorption line at low e-h density continuously turns to the broad absorption-gain spectra of e-h plasma at high e-h density, which is nothing but the exciton-Mott crossover. The excitonic peak is almost unshifted as in the PL spectra until the optical gain appears at around the energy of the new peak found in PL spectra. They also confirmed the thermalization of e-h systems by examining the Kubo-Martin-Schwinger (or Kennard-Stepanov) relation between the absorption-gain and PL spectra.[58] This relation does hold in wide range of the e-h density, and the temperatures were estimated roughly as 40–70 K, which is much higher than that of the environment ($\sim$4 K).[59]

Theoretically, the interaction effects in quasi-1D e-h systems are still controversial.[39,60–69] It is known in three dimensions that the perturbation theory or the equation of motion (so-called semiconductor Bloch equation) are quite effective,[2–10] in which the self-energy is evaluated via the screened Hartree-Fock approximation and the optical susceptibility is computed with the screened T matrix to include the excitonic correlation. However, in the quasi-1D system, their results depend quite severely on the treatment of the screening effects; if only the static screening is taken into account,[62–65] the sharp excitonic absorption line continuously transforms to the absorption-gain spectra of e-h plasma with increasing e-h density, which is accompanied by the red-shift of the

excitonic peak. Then, although the optical gain is correctly reproduced at high e-h density, the red-shift contradicts with the experimental observations. By contrast, if the dynamical screening is considered,[39] we see only the broadening of the unshifted excitonic peak as e-h density is increased. The optical gain is almost washed out by the strong intercarrier scatterings, which do not explain the recent experiments, again.

In the above theories,[39,62–65] they deal with an e-h pair embedded in the background of *e-h plasma*, taking into account the band-gap renormalization (BGR), screening and Pauli-blocking effects. The renormalized band gap monotonously decreases as the e-h density is increased. The energy shift of the excitonic bound state is much smaller owing to its charge neutrality. At the merging point of these two energies, i.e., at the *Mott density*, the excitonic bound state completely vanishes, and the optical gain can appear at low temperature where the population inversion of the e-h plasma is realized. Although this kind of theory does give an intelligible picture of the *exciton-Mott crossover*, its application to the regime of low e-h density and low temperature is problematic. For example, it does not explain the experimentally observed strong suppression of BGR. One can develop instead a self-consistent theory for an e-h pair embedded in the background of *exciton gas*, which correctly predicts BGR suppression at the low e-h density and low temperature.[70] However, at a certain e-h density, it shows a sudden collapse of excitonic bound states (*pure Mott transition* or *ionization catastrophe*), not the exciton-Mott crossover.

To overcome the above problem, and to obtain a unified description of the exciton-Mott physics, we need a treatment for an e-h pair embedded in the *mixture of exciton gas and e-h plasma*, and consider the *ionization ratio* in this mixture.[71] In terms of Green's function formalism, the e-h T matrix, which denotes the effects by the excitonic bound states, should be taken into account in the electron and the hole self-energies.[3,9,10,66–69,72–83] In a previous paper,[84] we developed a self-consistent screened T-matrix approximation, in which the self-energies, the screening parameter, and the T matrices are all determined in a consistent manner. Although the prototype of this approximation was already proposed more than two decades ago,[3,75,76] its application has been restricted only to the simplified theoretical models. Only recently, it is implemented for the realistic models of semiconductors.[77–83] Theories based on the equation-of-motion approach[85,86] and the path-integral Monte Carlo simulations[86,87] are also proposed to treat the exciton-plasma mixture, whereas the physical meaning of the ionization ratio is different from those used conventionally in the self-consistent T-matrix theories.[88]

The main purpose of this article is to understand the exciton-Mott crossover and the interband optical response in quasi-1D e-h systems, whereas, we also complete the discussions on the exciton-Mott transition. Two possibilities are pointed out regarding the exciton-Mott transition. One is the *gas-liquid transition* accompanied by a coexisting region of exciton gas and e-h plasma,[3,9–15,17,18] which are in fact observed in bulk indirect semiconductors, e.g., Si and Ge,[89] as well as in the type-II structures on direct semiconductors.[90] Inside the coexisting region, the e-h chemical potential (the sum of electron and hole chemical potentials) becomes independent of e-h density. The other one is the *pure Mott transition* characterized by the discontinuous jump of the ionization ratio.[19,23,70] This type of transition was observed recently in the coupled quantum wells (e-h bilayer),[91] which is, however, only poorly examined theoretically. Note that the exciton-Mott crossover and transition is distinctly distinguished here, while in some literature their difference is only ambiguously discussed.

Aside from the Mott transition, we can also imagine the quantum condensation (e-h pairings).[20–30] Since the e-h pairing is suppressed by the strong quantum fluctuations, it will be hard to see the real quantum condensation in quasi-1D systems. However, we still find its precursor effects in the single-particle spectra, as will be discussed in Sec. III E.

The paper is organized as follows: In Sec. II, we introduce the model Hamiltonian of the quantum wire, and explain our theoretical framework. Then, we present the results on the quasiequilibrium properties and on the optical response of quasi-1D e-h systems in Sec. III. Discussions and summaries are given in Secs. IV and V.

II. FORMULATION

A. Model of quasi-1D e-h system on quantum wire

We consider a model quantum wire along the x axis. Electrons and holes are confined in its rectangular cross section $|y| \leqslant \ell_y/2$, $|z| \leqslant \ell_z/2$ by a hard-wall potential. Under the sufficiently strong potential confinement, one is allowed to consider only the lowest subband, where the wave function in the confined directions reads as

$$u(\boldsymbol{r}_\perp) = \frac{2}{\sqrt{\ell_y \ell_z}} \cos\left(\frac{\pi}{\ell_y} y\right) \cos\left(\frac{\pi}{\ell_z} z\right) \tag{1}$$

with $\boldsymbol{r}_\perp = (y,z)$. Then, the effective electron-electron (e-e) Coulomb interaction potential along the wire is described in the Fourier transformed form

$$V_q = \frac{2e^2}{\varepsilon_0} \int_D d^2\boldsymbol{r}_\perp \int_D d^2\boldsymbol{r}'_\perp K_0(q|\boldsymbol{r}_\perp - \boldsymbol{r}'_\perp|) \times |u(\boldsymbol{r}_\perp)|^2 |u(\boldsymbol{r}'_\perp)|^2, \tag{2}$$

where D denotes the cross section of the quantum wire, ε_0 is the background dielectric constant, and $K_0(x)$ is the lowest-order modified Bessel function of the second kind.

It should be mentioned here that the lowest-subband approximation in Eq. (2) does not hold well in the T-shape quantum wire used in experiments.[47,54–57] The confinement potential in the T-shape quantum wire is rather shallow, and the effects of the excited subbands are non-negligible especially for the holes, namely, the intersubband energy spacing is smaller than the exciton binding energy. However, as we see shortly, ℓ_y and ℓ_z are tuned so as to reproduce the exciton binding energy observed in the experiments, so that the energy structures of the single-particle and optical spectra can be captured properly, even if Eq. (2) is used as the model interaction potential. Still, the spectral broadening induced by the intercarrier scatterings might be overestimated because the intersubband screening generally "softens" the short-range part of the interaction.

The electrons and holes confined in this quantum wire are described by the many-body Hamiltonian

$$\mathcal{H} = \sum_{ak\sigma} \epsilon_{ak} c^{\dagger}_{ak\sigma} c_{ak\sigma} + \frac{1}{2L} \sum_{q} V_q : \rho_{c,q} \rho_{c,-q} : , \qquad (3)$$

where L is the wire length, and the pair of colons means the normal ordering of annihilation and creation operators between them. The operator $c_{ak\sigma}$ annihilates an electron or a hole with a wave number k and spin σ, depending on $a = \mathrm{e}$ and h, respectively. The charge density operator is also written as

$$\rho_{c,q} = \sum_{ak\sigma} z_a c^{\dagger}_{ak-q\sigma} c_{ak\sigma}, \qquad (4)$$

where z_a denotes the sign of particle charge ($z_{\mathrm{e}} = -1$, $z_{\mathrm{h}} = +1$). The energy dispersions of electron and hole along the wire are given as

$$\epsilon_{a,k} = \frac{\hbar^2 k^2}{2m_a} + \frac{E_{\mathrm{g}}}{2} \qquad (5)$$

with the bare band gap E_{g} and the effective mass m_a.

B. Self-consistent screened T-matrix approximation with feedback to screening

We explain here the self-consistent screened T-matrix approximation (SSTA) developed by the authors.[84] It enables us to treat the suppression of plasma screening by the formation of e-h bound states. The flowchart of our numerical calculation is given in Fig. 1, together with the corresponding Feynman diagrams. Throughout this section, we use the Planck units, i.e., $\hbar = 1$ and $k_{\mathrm{B}} = 1$. Green's functions, T matrices, and self-energies presented below are retarded ones.

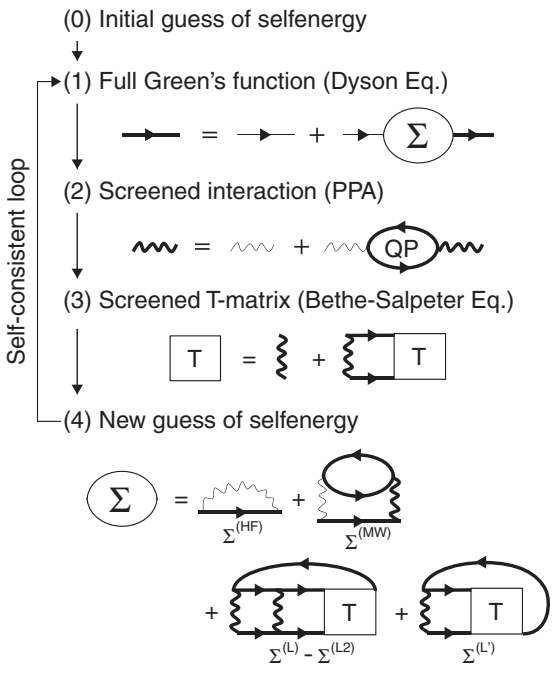

FIG. 1. Our calculation scheme depicted with Feynman diagrams. Thick and thin solid lines denote full and bare single-particle Green's functions, respectively, while thick and thin wavy lines represent screened and bare Coulomb interactions, respectively. Screening of interaction is evaluated with quasistatic plasmon pole approximation, considering only the quasiparticle contribution (ionized fraction).

Let us start from an initial guess of the self-energy $\Sigma_a(k,\omega)$. The full single-particle Green's function is written as

$$G_a(k,\omega) = \frac{1}{\omega - \epsilon_{a,k} + \mu_a - \Sigma_a(k,\omega)}. \qquad (6)$$

The chemical potential of the electron and hole, μ_{e} and μ_{h}, are determined so as to satisfy

$$n = -\frac{2}{L} \sum_{k} \int \frac{d\omega}{\pi} f_{\mathrm{F}}(\omega) \mathrm{Im} G_a(k,\omega), \qquad (7)$$

where n is the (axial) e-h density, i.e., electron, or equivalently, hole number per unit length on the wire, and $f_{\mathrm{F}}(\omega) = [e^{\omega/T} + 1]^{-1}$ is the Fermi distribution function at temperature T. The factor 2 stems from the spin degeneracy.

The energies of the quasielectron and the quasihole, $\xi_{\mathrm{e},k}$ and $\xi_{\mathrm{h},k}$, are given as the solution of

$$\mathrm{Re}\left[G_a^{-1}(k, \xi_{a,k} - \mu_a)\right] = 0, \qquad (8)$$

which determines the renormalized band gap

$$E^*_{\mathrm{g}} = \xi_{\mathrm{e},k=0} + \xi_{\mathrm{h},k=0}, \qquad (9)$$

and the quasiparticle densities

$$n^{(0)}_a = \frac{2}{L} \sum_{k} f_{\mathrm{F}}(\xi_{a,k} - \mu_a). \qquad (10)$$

Following the proposal by Zimmermann and Stolz,[75,76] we define the ionization ratio as

$$\alpha = \frac{1}{2n}\left(n^{(0)}_{\mathrm{e}} + n^{(0)}_{\mathrm{h}}\right), \qquad (11)$$

which denotes the e-h portion behaving like free particles.

The screening effect is taken into account via the plasmon-pole approximation. We evaluate the quasistatically screened Coulomb interaction potential as

$$W_q = V_q \left(1 + \frac{\Omega_q^2}{\Omega^2 - \overline{\Omega}_q^2}\right)\Bigg|_{\Omega \to 0} = V_q \left[1 + V_q \left[\frac{e^2}{\varepsilon_0 \kappa} + \frac{Cq^2}{16mn}\right]^{-1}\right]^{-1}, \qquad (12)$$

using the quasi-1D plasma frequency

$$\Omega_q = \left[\frac{nq^2}{m} V_q\right]^{1/2} \qquad (13)$$

and the effective plasmon-pole frequency

$$\overline{\Omega}_q = \left[\Omega_q^2 + \frac{ne^2}{\varepsilon\kappa} \cdot \frac{q^2}{m} + \frac{Cq^4}{16m^2}\right]^{1/2}, \qquad (14)$$

where κ is the (dimensionless) screening parameter and C is the adjustable parameter introduced to describe the contribution other than the plasmon pole.[62] We expect that the screening is mostly attributable to the e-h plasma, and is determined by $n^{(0)}_{\mathrm{e}} \sim n^{(0)}_{\mathrm{h}}$. Thus, we estimate the screening

parameter as

$$\kappa = \frac{2\lambda_{\rm L}}{L}\sum_{a,k} f_{\rm F}(\xi_{a,k}-\mu_a)[1-f_{\rm F}(\xi_{a,k}-\mu_a)] \tag{15}$$

using the so-called Landau length $\lambda_{\rm L} = e^2/\varepsilon_0 T$. Here, only the quasiparticle contribution is kept, and the interaction between the quasiparticles is neglected. We adopt $C = 4$ following Ref. 62, while the final results depend only weakly on the value of C.

Next, we evaluate the screened T matrices $\mathcal{T}_{ab}(k,k';Q,\Omega)$, in order to consider the multiple e-e ($a = b =$ e), h-h ($a = b =$ h), and e-h ($a \neq b$) scatterings in which the wave numbers of a and b particles are changed from k and $Q-k$ to k' and $Q-k'$, respectively. Among them, the e-h one, $\mathcal{T}_{\rm eh}$, is especially important since it describes the effects of the excitonic bound states. These T matrices are determined so as to satisfy the Bethe-Salpeter equation

$$\begin{aligned}&\mathcal{T}_{ab}(k,k';Q,\Omega)\\ &\quad = z_a z_b W_{|k-k'|} + \frac{1}{L}\sum_{k''} z_a z_b W_{|k-k''|}\mathcal{G}^{(0)}_{ab}(k'';Q,\Omega)\\ &\qquad\times \mathcal{T}_{ab}(k'',k';Q,\Omega).\end{aligned} \tag{16}$$

Here, the pair Green's function without vertex correction is expressed in the spectral representation as

$$\mathcal{G}^{(0)}_{ab}(k;Q,\Omega) = -\int\frac{d\Omega'}{\pi}\frac{{\rm Im}\mathcal{G}^{(0)}_{ab}(k;Q,\Omega')}{\Omega-\Omega'+i\delta} \tag{17}$$

with

$$\begin{aligned}&{\rm Im}\mathcal{G}^{(0)}_{ab}(k;Q,\Omega)\\ &\quad = -\int\frac{d\omega'}{\pi}[1-f_{\rm F}(\omega')-f_{\rm F}(\Omega-\omega')]\\ &\qquad\times {\rm Im}G_a(k,\omega'){\rm Im}G_b(Q-k,\Omega-\omega')\end{aligned} \tag{18}$$

$$\begin{aligned}&\quad = -\frac{1}{f_{\rm B}(\Omega)}\int\frac{d\omega'}{\pi}f_{\rm F}(\omega')f_{\rm F}(\Omega-\omega')\\ &\qquad\times {\rm Im}G_a(k,\omega'){\rm Im}G_b(Q-k,\Omega-\omega'),\end{aligned} \tag{19}$$

where δ is an infinitesimally small positive number, and $f_{\rm B}(\Omega) = [e^{\Omega/T}-1]^{-1}$ is the Bose distribution function. Two Fermi distribution functions in Eq. (18) account for the Pauli-blocking effects on the electron and hole, respectively.

Then, the new guess of the self-energy is given in the spectral representation as

$$\Sigma_a(k,\omega) = \Sigma^{\rm (HF)}_a(k) - \int\frac{d\omega'}{\pi}\frac{{\rm Im}\Sigma_a(k,\omega')}{\omega-\omega'+i\delta}, \tag{20}$$

with the Hartree-Fock self-energy

$$\Sigma^{\rm (HF)}_a(k) = \frac{1}{L}\sum_{k'} V_{|k-k'|}\int\frac{d\omega}{\pi}{\rm Im}G_a(k',\omega). \tag{21}$$

The imaginary part of the self-energy, which denotes the correlation effects, is decomposed into four terms:

$${\rm Im}\Sigma_a = {\rm Im}\big[\Sigma^{\rm (MW)}_a - \Sigma^{\rm (L2)}_a + \Sigma^{\rm (L)}_a + \Sigma^{\rm (L')}_a\big]. \tag{22}$$

Here, $\Sigma^{\rm (MW)}_a$ and $\Sigma^{\rm (L2)}_a$ denote the Montroll-Ward[9,10] and the screened Born (the second-order contribution of $\Sigma^{\rm (L)}_a$) terms, respectively, while $\Sigma^{\rm (L)}_a$ and $\Sigma^{\rm (L')}_a$ describe the direct and exchange contributions of the screened T matrix, respectively. Their contributions are explicitly written as

$$\begin{aligned}&{\rm Im}\big[\Sigma^{\rm (MW)}_a(k,\omega) - \Sigma^{\rm (L2)}_a(k,\omega)\big]\\ &\quad = -\int\frac{d\omega'}{\pi}[f_{\rm B}(\omega+\omega')+f_{\rm F}(\omega')]\\ &\qquad\times\frac{2}{L^2}\sum_{b,k'k''}(V_{|k-k''|}-W_{|k-k''|})W_{|k-k''|}\\ &\qquad\times {\rm Im}\mathcal{G}^{(0)}_{ab}(k'';k+k',\omega+\omega'){\rm Im}G_b(k',\omega')\end{aligned} \tag{23}$$

and

$$\begin{aligned}&{\rm Im}\big[\Sigma^{\rm (L)}_a(k,\omega) + \Sigma^{\rm (L')}_a(k,\omega)\big]\\ &\quad = -\int\frac{d\omega'}{\pi}[f_{\rm B}(\omega+\omega')+f_{\rm F}(\omega')]\\ &\qquad\times\frac{1}{L}\sum_{b,k'}{\rm Im}[2\mathcal{T}_{ab}(k,k;k+k',\omega+\omega')\\ &\qquad-\delta_{ab}\mathcal{T}_{aa}(k,k';k+k',\omega+\omega')]{\rm Im}G_b(k',\omega'),\end{aligned} \tag{24}$$

where the factor 2 again results from the spin degeneracy.[93]

The self-energy contribution of Eq. (23) is rather irrelevant since the screening is suppressed in quasi-1D systems: $V_k \sim W_k$. Therefore, the self-energies are almost dominated by the T-matrix contribution $\Sigma^{\rm (L)}$, which expresses the effects of the excitonic bound states and of the multiple intercarrier scatterings. Particularly, the latter effect leads to *intrinsic broadening* in the single-particle and optical spectra. This makes sharp contrast to the theory of the semiconductor Bloch equation, the self-energy of which does not include these effects, and the spectral broadening can be treated phenomenologically at best (see Sec. II D for details).

Starting with an initial guess of $\Sigma_a(k,\omega)$, we iterate the above loop of calculation until it converges. Then, we eventually determine the self-energy $\Sigma_a(k,\omega)$, the screening parameter κ, and the T matrix $\mathcal{T}_{ab}(k,k';Q,\Omega)$, which are consistent with each other.

Our formalism is overall based on Ref. 77, but has distinctive difference in the following points. One is the improvement in the definition of the ionization ratio. We consider that our definition by Eqs. (10) and (11) is more reasonable because the one used in Ref. 77 sometimes gives a considerable difference between $n^{(0)}_{\rm e}$ and $n^{(0)}_{\rm h}$. Another difference lies in the self-energy terms. We substitute the second-order scattering (screened Born) term in the direct T-matrix contribution with the Montroll-Ward term to avoid double counting of Feynman diagrams. We no longer need the additional screened Hartree-Fock (SHF) term, namely, the sum of the static screened-exchange and the Coulomb-hole terms, since it is already considered via the Hartree-Fock and the Montroll-Ward terms. We also add the exchange contributions of T matrices neglected in Ref. 77.

Our SSTA fully takes into account the two-body (excitonic) correlations via the T matrices. Thus, it is valid in the low e-h density region except at the extremely low temperature where the trionic (three-body) or the biexcitonic (four-body) correlations are relevant. Meanwhile, in the high e-h density region, our SSTA is valid again, where the Montroll-Ward self-energies play the most essential role and the T-matrix

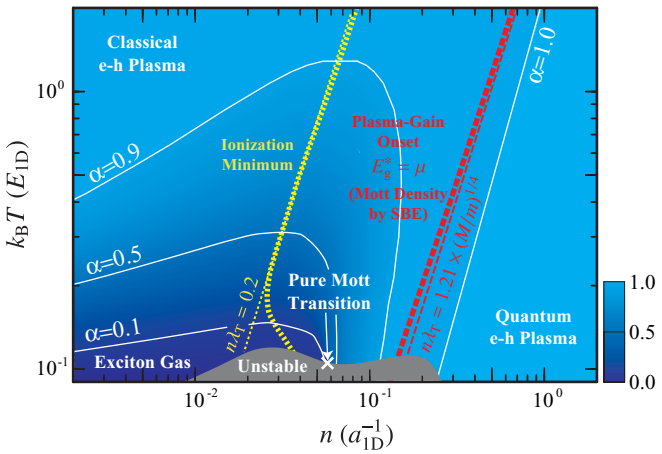

FIG. 2. (Color online) Phase diagram of quasi-1D e-h system depicted as intensity plot of ionization ratio α on the n-T plane. Electron-hole density n and temperature T are scaled by inverse of quasi-1D exciton Bohr radius $a_{1D}^{-1} = (8.09\ \text{nm})^{-1} = 1.24 \times 10^{-6}\ \text{cm}^{-1}$, and binding energy $E_{1D} = 14.0\ \text{meV} = 162\ \text{K}$, respectively. Isothermal compressibility diverges at the boundary of the gray-shaded region, inside which an inhomogeneous thermodynamic state is expected. This boundary shows a dip near $na_{1D} \sim 6 \times 10^{-2}$, on which there is a pure Mott transition point. Thin solid lines denote the contours of $\alpha = 0.1$, 0.5, 0.9, and 1.0. On the thick dotted line, ionization ratio has its minimum at the fixed temperature, and starts to show quantum dissociation of quasiexcitons. This line almost overlaps the thin dotted line expressed by Eq. (44). Thick and thin broken lines show the plasma-gain-onset densities evaluated by our SSTA and by Eq. (28), respectively. Equation (28) also gives a good approximation for the Mott density evaluated by the semiconductor Bloch equation (SBE).

contributions become irrelevant. Therefore, our SSTA is expected to give a reasonable interpolation between the low and the high e-h density regimes, and enables us to draw a "global" phase diagram of e-h systems, as will be shown in Fig. 2.

Although the quasistatically screened interaction is used in the T matrices, the dynamical correlation effects are still taken into account in our SSTA. As already discussed in Ref. 39, the most essential consequence of the dynamical screening is the ω dependence of the screened HF self-energies at intermediate or high e-h densities. In our SSTA, this ω dependence is included in the Montroll-Ward terms, so that the dynamical screening effect is accounted for partially. In the previous theories, the dynamical screening effects in the T matrices are completely neglected,[62–64] or treated only approximately,[39,65] in order to carry out the numerical evaluation. It is known that some of the approximations to the dynamically screened T matrices give unphysical results. For example, the so-called Shindo approximation[92] seems to hide the optical gain observed experimentally.[39]

C. Interband optical spectra

Now, let us consider the interband optical response against the linearly polarized light along the quantum wire, neglecting the wave-number dependence of the corresponding dipole matrix element d. The optical absorption-gain spectra, i.e., the imaginary part of the interband optical susceptibility per unit length, is written as

$$P_{\text{abs}}(\Omega) = -\frac{2|d|^2}{L}\text{Im}\left[\sum_{kk'}\mathcal{G}_{\text{eh}}(k,k';Q=0,\Omega-\mu)\right], \quad (25)$$

as a function of the photon energy Ω, where the e-h chemical potential is defined as $\mu = \mu_e + \mu_h$, and the full e-h pair Green's function is given as

$$\begin{aligned}\mathcal{G}_{\text{eh}}(k,k';Q,\Omega) &= \mathcal{G}^{(0)}_{\text{eh}}(k;Q,\Omega)\delta_{kk'} \\ &\quad + \frac{1}{L}\mathcal{G}^{(0)}_{\text{eh}}(k;Q,\Omega)\mathcal{T}_{\text{eh}}(k,k';Q,\Omega)\mathcal{G}^{(0)}_{\text{eh}}(k';Q,\Omega). \quad (26)\end{aligned}$$

The photoluminescence spectra can also be obtained from these absorption-gain spectra by means of the Kubo-Martin-Schwinger (KMS) relation. In fact, they are proportional to

$$P_{\text{PL}}(\Omega) = f_{\text{B}}(\Omega-\mu)P_{\text{abs}}(\Omega). \quad (27)$$

Note that KMS relation holds exactly under our SSTA.[77,93]

The KMS relation and the inequality $P_{\text{PL}}(\Omega) \geqslant 0$ also show that the optical absorption is possible at $\Omega > \mu$, while the optical gain (negative absorption) appears at $\Omega < \mu$. Therefore, the e-h plasma (quasielectrons and quasiholes) can contribute to the gain at the high-n region satisfying $E_g^* \leqslant \mu$. With this in mind, we determine the *plasma-gain-onset density* $n_P(T)$ by the condition, $E_g^* = \mu$ at a given temperature T. As will be discussed in the Appendix, we find a simple approximation for this density:

$$n_P\lambda_T \sim 2\left(\frac{M}{m}\right)^{1/4} I_{-1/2}(0) = 1.21 \times \left(\frac{M}{m}\right)^{1/4}, \quad (28)$$

where we define the thermal de Broglie wavelength as

$$\lambda_T = \frac{h}{\sqrt{2\pi m k_B T}} \quad (29)$$

with the *reduced mass* m. This formula shows that the plasma-gain onset can be understood as a classical-quantum crossover. In other words, it is essentially determined by the Pauli-blocking or the phase-space-filling effects and is insensitive to the many-body effects, e.g., the screening. This fact gives the reason why the free-carrier theory explains some aspects of the experimental observations pretty well.

The real part of the the interband optical susceptibility also gives the information on the e-h pair condensation. In fact, the e-h pair susceptibility

$$\chi_{\text{pair}} = \frac{2}{L}\sum_{kk'}\mathcal{G}_{\text{eh}}(k,k';Q=0,\Omega=0) \quad (30)$$

should diverge at the critical temperature or at the critical density if the e-h pair condensation takes place. This is the so-called Thouless criterion.[30,94]

D. Semiconductor Bloch equation

In the following sections, we compare the results obtained by our SSTA with those by the so-called semiconductor Bloch equation (SBE).[62–64] In the SBE, one considers a pair of a quasielectron and a quasihole embedded in the pure e-h

plasma. The finite-lifetime effects of the quasielectron and quasihole are neglected, and only their renormalizations in energy are taken into account. It is examined whether this pair can form a bound state (quasiexciton) or not by considering the screening of e-h attractive interaction and the Pauli-blocking effect.

The SBE considers the renormalization of the electron and the hole energies by means of the screened Hartree-Fock approximation (SHFA). The quasiparticle energies $\xi_{a,k}$ and the chemical potential μ_a are determined so as to satisfy

$$\xi_{a,k} = \epsilon_{a,k} + \frac{1}{2}\sum_q (W_q - V_q) - \sum_{k'} W_{k-k'} f_{\rm F}(\xi_{a,k'} - \mu_a), \tag{31}$$

$$\kappa = \frac{2\lambda_{\rm L}}{L}\sum_{a,k} f_{\rm F}(\xi_{a,k} - \mu_a)[1 - f_{\rm F}(\xi_{a,k} - \mu_a)], \tag{32}$$

$$n = \frac{2}{L}\sum_k f_{\rm F}(\xi_{a,k} - \mu_a), \tag{33}$$

where the screened interaction potential W_q is evaluated by substituting Eq. (32) into Eq. (12). The second and the third terms of Eq. (31) are called Coulomb hole and screened exchange self-energies, respectively. The renormalized band gap $E_{\rm g}^*$ is also determined via Eq. (9).

The single-particle Green's function is approximated in the free-carrier form as

$$G_a(k,\omega) \sim \frac{1}{\omega - \xi_{a,k} + \mu_a + i\delta}. \tag{34}$$

Then, Eqs. (16)–(18), and (26) lead to the formal expression of the full e-h pair Green's function[95,96]

$$\hat{\mathcal{G}}_{\text{e-h}}(Q,\Omega) = (\Omega - \hat{H}_Q + \mu + i\delta)^{-1}\hat{F}_Q. \tag{35}$$

Here, we use the matrix notation: the matrix elements of $\hat{\mathcal{G}}_{\text{e-h}}(Q,\Omega)$ are given by $\mathcal{G}_{\text{e-h}}(k,k';Q,\Omega)$, and the effective Hamiltonian for the quasielectron-quasihole pair with the total momentum Q is defined as

$$\hat{H}_Q = \hat{K}_Q - \frac{1}{L}\hat{F}_Q\hat{W}. \tag{36}$$

The matrix elements of $\hat{K}_Q$, $\hat{F}_Q$, and $\hat{W}$ are written as

$$[\hat{K}_Q]_{kk'} = (\xi_{{\rm e},k} + \xi_{{\rm h},Q-k})\delta_{kk'}, \tag{37}$$

$$[\hat{F}_Q]_{kk'} = [1 - f_{\rm F}(\xi_{{\rm e},k} - \mu_{\rm e}) - f_{\rm F}(\xi_{{\rm h},Q-k} - \mu_{\rm h})]\delta_{kk'}, \tag{38}$$

$$[\hat{W}]_{kk'} = W_{k-k'}, \tag{39}$$

respectively. Equation (35) is numerically evaluated by diagonalizing $\hat{H}_Q$. Although $\hat{H}_Q$ is not Hermite due to $(\hat{F}_Q\hat{W})^\dagger = \hat{W}\hat{F}_Q \neq \hat{F}_Q\hat{W}$, we can prove that all eigenvalues of $\hat{H}_Q$ are real. If the lowest eigenvalue of $\hat{H}_{Q=0}$ lies below the renormalized band gap $E_{\rm g}^*$, it can be identified as the (ground) energy of quasiexciton $E_{\rm X}^*$.

In the SBE framework, the exciton Mott crossover is discussed traditionally in terms of the *Mott density* $n_{\rm M}(T)$, which is determined by the condition $B_{\rm X}^* = E_{\rm g}^* - E_{\rm X}^* \to +0$ at a given temperature T. As n is increased, both the Coulomb hole and the screened exchange self-energies work to reduce the effective band gap $E_{\rm g}^*$. Whereas, the quasiexciton energy $E_{\rm X}^*$ shows much weaker dependence on n owing to its charge neutrality. This means that the effective binding energy $B_{\rm X}^*$ is suppressed by the Pauli-blocking and the screening effects. At the Mott density, the quasiexciton level $E_{\rm X}^*$ finally merges into the energy continuum of scattering states above $E_{\rm g}^*$, which implies the complete ionization of the excitons.

Now, let us discuss the relation between the Mott and the plasma-gain-onset densities within the SBE framework. In the following, for a given temperature T, we assume that phase transitions never occur at any e-h densities. This leads to $\mu < E_{\rm X}^*$ at $n < n_{\rm M}(T)$ since $\mu \to E_{\rm X}^* - 0$ implies the divergence of the e-h pair susceptibility, or equivalently, the e-h pair condensation. Then, we obtain the inequality $n_{\rm M}(T) \leqslant n_{\rm P}(T)$ because $\mu < E_{\rm X}^* < E_{\rm g}^*$ and thus $n < n_{\rm P}(T)$ always hold as far as $n < n_{\rm M}(T)$ is fulfilled. Here, it should be noted that the conditions $n < n_{\rm M}(T)$ and $n < n_{\rm P}(T)$ are equivalent to $E_{\rm X}^* < E_{\rm g}^*$ and $\mu < E_{\rm g}^*$, respectively.

Further, we can show the equality $n_{\rm M}(T) = n_{\rm P}(T)$ in 1D and 2D e-h systems, as shown in the following. This is a direct consequence of the stability of bound states, and is one of the characteristic aspects of the low-dimensional e-h systems. The proof is simple. At $n < n_{\rm P}(T)$, the Pauli-blocking factor $\hat{F}_Q$ is a positive definite. In fact, we can confirm the inequality

$$1 - f_{\rm F}(\xi_{{\rm e},k} - \mu_{\rm e}) - f_{\rm F}(\xi_{{\rm h},Q-k} - \mu_{\rm h}) = \frac{f_{\rm F}(\xi_{{\rm e},k} - \mu_{\rm e}) f_{\rm F}(\xi_{{\rm h},Q-k} - \mu_{\rm h})}{f_{\rm B}(\xi_{{\rm e},k} + \xi_{{\rm h},Q-k} - \mu)} > 0 \tag{40}$$

since $\xi_{{\rm e},k} + \xi_{{\rm h},Q-k} \geqslant E_{\rm g}^* > \mu$. Thus, we can define $\hat{F}_Q^{1/2}$ and the similar matrix

$$\hat{H}'_Q = \hat{F}_Q^{-1/2}\hat{H}_Q\hat{F}_Q^{1/2} = \hat{K}_Q - \frac{1}{L}\hat{F}_Q^{1/2}\hat{W}\hat{F}_Q^{1/2}, \tag{41}$$

which is Hermite and has the same eigenvalues as $\hat{H}_Q$. As a result, the problem is mapped to an ordinary Schrödinger equation for the e-h pair with an effective attractive interaction. Note that even an infinitesimally small attractive potential can form a bound state in 1D and 2D systems,[97] so that a quasiexciton always exists at $n < n_{\rm P}(T)$, which implies $n_{\rm M}(T) \geqslant n_{\rm P}(T)$. As mentioned above, the converse inequality, $n_{\rm M}(T) \leqslant n_{\rm P}(T)$, generally holds. Thus, we finally obtain the equality.

As Mott himself argued, the screening effect plays the most essential role in the Mott physics in the bulk (three-dimensional) e-h systems: the quasiexcitons are expected to be dissociated when the exciton Bohr radius becomes comparable to the screening length. Therefore, the above equality $n_{\rm M}(T) = n_{\rm P}(T)$ might seem peculiar since it means that not only the plasma-gain-onset density but the Mott density is determined almost only by the Pauli-blocking effect. However, we should note that Mott's argument holds only in the bulk case. At low dimensions, the quasiexciton is never dissociated only by the screening effects since a bound state survives even for an infinitesimally weak e-h attractive interaction.

Not only in our SSTA, but also in the SBE framework, the plasma-gain-onset density $n_{\rm P}(T)$ is well approximated by Eq. (28). Thus, for quasi-1D e-h systems, we finally obtain

$$n_{\rm M}(T) = n_{\rm P}(T) \sim 1.21 \times \left(\frac{M}{m}\right)^{1/4}\frac{1}{\lambda_{\rm T}}. \tag{42}$$

III. RESULTS

The parameter values in our model are chosen with in mind the T-shape quantum wires used in the recent experiment,[47,54–57] which are fabricated at the intersection of a 14 nm (001) $Al_{0.07}Ga_{0.93}As$ and 6 nm (110) GaAs quantum wells. Using the effective masses of bulk GaAs along the wire,[64] we estimate the electron and hole effective masses as $m_e = 0.0665m_0$ and $m_h = 0.11m_0$, respectively, where m_0 denotes the electron rest mass. Then, the exciton total and reduced masses are given by $M = m_e + m_h = 0.1765m_0$ and $m = m_e m_h/(m_e + m_h) = 0.0414m_0$, respectively. We optimize the side lengths of the rectangular cross section, ℓ_y and ℓ_z, so as to reproduce the experimentally observed quasi-1D exciton binding energy $E_{1D} = 14.0$ meV by fixing the aspect ratio to $\ell_z/\ell_y = 6/14$, and using the background dielectric constant $\varepsilon_0 = 13.74$. This evaluation gives $\ell_z/a_{1D} = 1.00$, where we define the quasi-1D Bohr radius as $a_{1D} = \hbar/\sqrt{2mE_{1D}} = 8.09$ nm.

Hereafter, all the energy and length quantities are scaled by E_{1D} and a_{1D}, respectively. The results are insensitive to ℓ_z/ℓ_y, as well as to ℓ_z/a_{1D}, while their temperature dependence is affected by the e-h mass ratio m_e/m_h to some extent.

A. Phase diagram

Before discussing the single-particle and interband optical spectra in the quasi-1D e-h system, we give an overview of exciton-Mott physics. The phase diagram on the n-T plane is given in Fig. 2, which is depicted as an intensity plot of ionization ratio α. This diagram clearly shows that the traditionally used Mott density gives only an oversimplified description of the exciton-Mott physics.

The electrons and holes are almost fully ionized and behave as classical and quantum plasma in the left-upper (low-n and high-T) region and the right-lower (high-n and low-T) region, respectively. Almost pure exciton gas, characterized by the extremely small ionization ratio, is realized only at low e-h density ($na_{1D} \lesssim 0.5 \times 10^{-1}$) and low temperature ($k_BT/E_{1D} \lesssim 10^{-1}$). At even lower temperature, there is a shaded region in which we find the homogeneous thermodynamic states being unstable. Its boundary is determined by the divergence of the isothermal compressibility

$$-\frac{1}{L}\left(\frac{\partial L}{\partial p}\right)_T = \frac{1}{n^2}\left(\frac{\partial \mu}{\partial n}\right)_T^{-1} \to +\infty, \tag{43}$$

where p denotes the "pressure" of the e-h system. The stability of the homogeneous thermodynamic state requires that μ is an increasing function of n. Therefore, the above divergence implies the instability toward either a phase separation or an inhomogeneous thermodynamic state. This boundary shows a dip at around $na_{1D} \sim 6 \times 10^{-2}$, which is a pure Mott transition point, namely, one finds there a discontinuity in the ionization ratio as a function of e-h density.

On the thick dotted line, the ionization ratio shows the minima at the fixed temperatures. This line almost overlaps the thin dotted line which expresses the condition

$$n\lambda_T \sim 0.2, \tag{44}$$

and thus defines a *classical-quantum crossover*. The physical meaning of this crossover is the onset of the quantum dissociation of the quasiexciton. In fact, as shown in the next section, the ionization is a rapidly increasing function of n in the quantum regime $n\lambda_T \gtrsim 0.2$, whereas it is a decreasing function of n in the classical regime $n\lambda_T < 0.2$, obeying the classical Saha equation.

The solid line shows the plasma-gain-onset density $n_P(T)$, at which the optical gain induced by e-h plasma appears satisfying the condition $\mu = E_g^*$. As discussed in Sec. II C, this density is well approximated by Eq. (28):

$$n\lambda_T \sim 1.21 \times (M/m)^{1/4} = 1.74, \tag{45}$$

as shown in the broken line. It provides the criterion of the *classical-quantum crossover* for the interband optical spectra, as will be mentioned in Sec. III D. This broken line almost coincides with the chain line which shows the Mott density obtained by the SBE. Let us remind here that the Mott and the plasma-gain-onset densities are exactly the same within the SBE framework, as proved in Sec. II D.

B. Thermodynamic quantities

Figure 3(a) represents the n dependence of the ionization ratio α at several temperatures. At low e-h density $n\lambda_T \ll 1$, the ionization ratio is well approximated by the Saha equation[3] for the mixture of ideal gas of electrons, holes, and excitons:

$$\frac{\alpha^2}{1-\alpha} = \frac{1}{n\lambda_T}\exp\left(-\frac{E_{1D}}{k_BT}\right). \tag{46}$$

This equation predicts the enhancements of α with increasing T or with decreasing n, which we call *entropy* and *thermal* dissociations,[98] respectively. The ionization ratio has its minimum at around the e-h density of Eq. (44) as indicated by arrows, and then starts to deviate from the classical Saha equation at the higher e-h density. Indeed, α is drastically increased as a function of n, which we call *quantum* dissociation.[98] This dissociation is caused by the reduction of the quasiexciton binding energy and the level broadening of the quasiexciton. At low temperature, this feature is enhanced and finally turns to a discontinuous jump on the pure exciton-Mott transition point. Discontinuous change at the transition point is also seen in the e-h chemical potential, screening parameter, and the band-gap renormalization, as will be mentioned shortly.

In Fig. 3(b), we plot the e-h chemical potential μ, as a function of n. At high temperature ($k_BT/E_{1D} \gtrsim 0.3$), μ gradually and monotonously increases as a function n. However, once we enter a low-temperature region, μ starts to show an anomaly at around $na_{1D} \sim 0.5$. As the temperature decreases, μ shows a stepwise increase from the value in the almost pure exciton gas to that in the quantum e-h plasma, as seen in the data at $k_BT/E_{1D} = 0.13$. This characteristic behavior is a precursor of the pure Mott transition. We also confirm that the e-h chemical potential at such low temperature approaches asymptotically the result for the ideal gas of exciton at low e-h densities, and not the one calculated by screened Hartree-Fock approximation, in which excitonic effects are neglected. The discontinuity in the e-h chemical potential is about a half of the exciton binding energy: $\Delta\mu \sim E_{1D}/2$. An explanation for this value of $\Delta\mu$ will be given in Sec. III C. Except for the stepwise

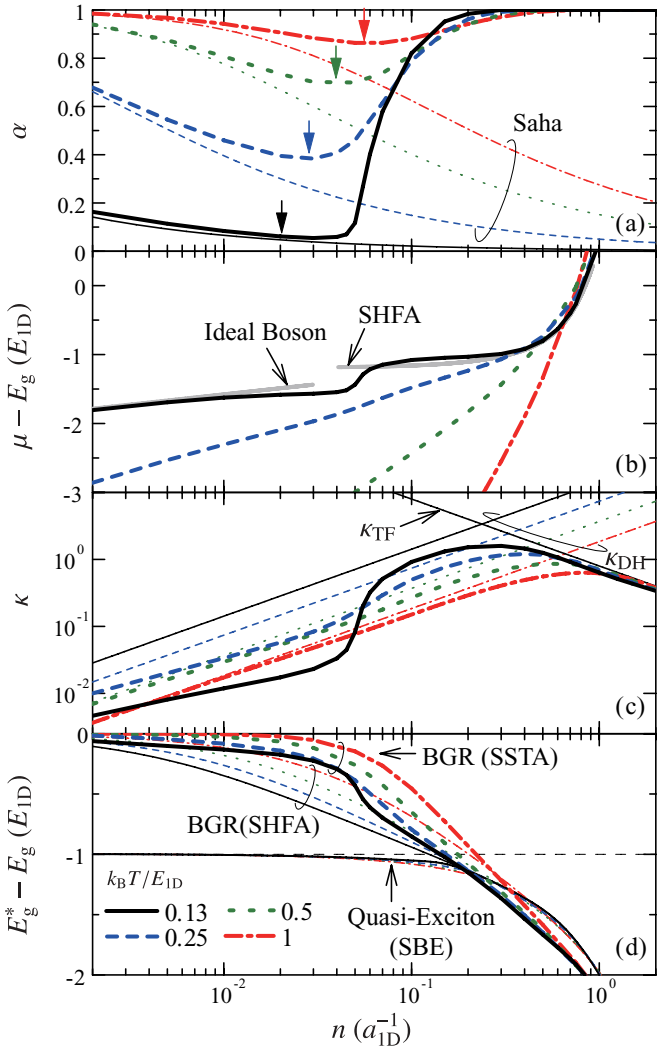

FIG. 3. (Color online) e-h density dependence of several single-particle quantities at $k_BT/E_{1D} = 0.13$, 0.25, 0.5, and 1. (a) e-h density dependence of ionization ratio α (thick lines), together with those evaluated by the Saha equation (thin lines). Arrows show the quantum-dissociation-onset density. (b) e-h chemical potential μ. Gray solid lines show results calculated in ideal exciton gas on the low e-h density side, and those obtained by screened Hartree-Fock approximation (SHFA) in the high e-h density side. (c) Screening parameter κ (thick lines) together with results calculated by Debye-Hückel and Thomas-Fermi approximations κ_{DH} and κ_{TF} (thin lines). (d) Band-gap renormalization $E_g^* - E_g$ (thick lines), together with those obtained by SHFA (thin lines). Quasiexciton energy estimated by SBE is also shown in the thin lines.

increase mentioned above, μ shows only weak n dependence, which is understood as the precursor of the instability toward the inhomogeneity [$(\partial\mu/\partial n)_T \to +0$ in Eq. (43)].

Figure 3(c) shows the n dependence of screening parameter κ. At high temperature, its asymptotic behaviors in the low and high e-h density limits are well described by the Debye-Hückel and Thomas-Fermi approximations

$$\kappa_{DH} = 2n\lambda_L = \frac{2e^2 n}{\varepsilon_0 k_B T}, \tag{47}$$

$$\kappa_{TF} = \frac{4M}{\pi m}\cdot\frac{2n\lambda_L}{(n\lambda_T)^2} = \frac{e^2}{\varepsilon_0}\frac{4M}{\pi^2\hbar^2 n}, \tag{48}$$

respectively. Our results interpolate these two limiting cases: κ monotonically increases at low e-h density, then takes a maximum at around the e-h density satisfying

$$n\lambda_T = \left(\frac{4M}{\pi m}\right)^{1/2}, \tag{49}$$

which is determined by $\kappa_{DH} = \kappa_{TF}$, and finally turns to a decreasing function at high e-h density. The condition of Eq. (49) gives the criterion of the classical-quantum crossover of the screening parameter. At low temperature, κ shows some singular behaviors at low e-h density. In fact, κ is strongly suppressed from κ_{DH} in the region with ionization ratio $\alpha \lesssim 0.6$. Resultantly, we see the drastic change of α near at $na_{1D} \sim 0.6$. In particular, we see a discontinuous shift of κ at the pure Mott transition point.

Figure 3(d) shows the n dependence of band-gap renormalization (BGR) $E_g^* - E_g$ for several choices of temperatures together with those obtained by SHFA. Our SSTA predicts that the BGR is much smaller than that of SHFA at the low-n region $n\lambda_T \lesssim 0.2$ where the quantum dissociation effect is irrelevant. This suppression of BGR is actually observed in experiments. In SHFA, BGR is mainly determined by the Coulomb hole term or, equivalently, by the screening by the e-h plasma in this low-n region, which gives rise to a relevant red-shift of E_g^*. By contrast, in our SSTA, the e-h T-matrix contribution, namely, the multiple e-h scattering effect, is dominant in the self-energy, which influences strongly the formation of the exciton satellite peak in the single-particle spectra, but affect BGR only weakly (see also Sec. III C).

At low temperature, the BGR is further reduced in our SSTA since the screening is suppressed by the exciton formation. As a result, it starts to show stepwise e-h density dependence at low temperature, reflecting the drastic change of ionization ratio at $na_{1D} \sim 5 \times 10^{-2}$. Above the plasma-gain-onset density, the deviation of BGR by our SSTA from that by the SHFA becomes smaller at all temperatures.

In Fig. 3(d), we also show the n dependence of the quasiexciton energy $E_X^* - E_g^*$, which is estimated by SBE and measured from the bare band gap. Its energy shifts are much smaller than those of BGR. Although SBE uses the SHFA self-energies which overestimate BGR at low e-h density, it well reproduces the excitonic peak energies of the PL spectra obtained by our SSTA (see Sec. III D). This insensitivity of quasiexciton energy to the treatment of the surrounding background (self-energies) stems from its charge neutrality. Only at around the Mott density, the quasiexciton energy is slightly red-shifted, merging into the energy continuum of the scattering states above E_g^*.

As mentioned above, the BGR $E_g^* - E_g$ is strongly suppressed in the low-n region. This suppression ends at some e-h density, and BGR starts to decrease distinctly as a function of n. Since the quasiexciton energy is almost independent of n, the quasiexciton binding energy $B_X^* = E_g^* - E_X^*$ is also reduced when n exceeds this e-h density. In other words, this e-h density corresponds to the classical-quantum crossover shown in the thick dotted line in Fig. 2, which gives the onset of quantum dissociation of excitons or, equivalently, the minimum of the ionization ratio. Actually, we can confirm that the ionization

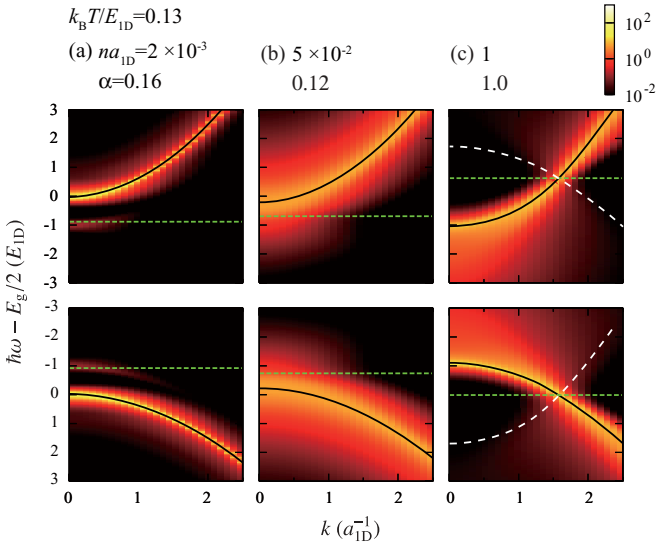

FIG. 4. (Color online) Intensity plots of single-particle spectral functions for electron (upper panel) and hole (lower panel) at a low temperature $k_BT/E_{1D} = 0.13$. Electron-hole densities are given as (a) $na_{1D} = 2 \times 10^{-3}$, (b) 5×10^{-2}, and (c) 1. Black solid lines represent quasielectron and hole energies $\xi_{e,k}$ and $\xi_{h,k}$. Chemical potentials of the electron and the hole are also shown in broken lines. White broken lines in (c) show the "shadow" dispersion of the quasihole and quasielectron energies $\mu - \xi_{h,k}$ and $\mu - \xi_{e,k}$.

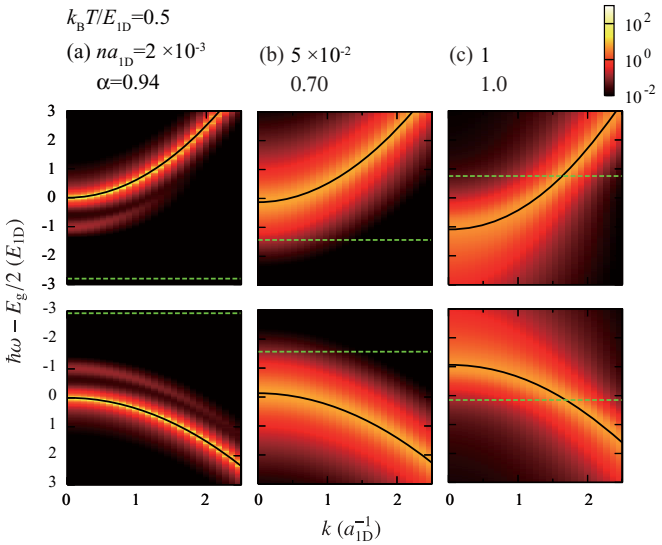

FIG. 5. (Color online) Intensity plots of single-particle spectral functions for electron and hole at a high temperature $k_BT/E_{1D} = 0.5$. Electron-hole densities are given as (a) $na_{1D} = 2 \times 10^{-3}$, (b) 5×10^{-2}, and (c) 1.

ratio has the minimum in Fig. 3(a) at the e-h density where the BGR curve is "bent" and starts to be decreased in Fig. 3(d).

C. Single-particle spectral functions

Figure 4 shows the single-particle spectra

$$A_a(k,\omega) = -2\,\mathrm{Im}G_a(k,\omega - \mu_a/\hbar) \quad (a = \mathrm{e,h}) \tag{50}$$

at low temperature for three different choices of e-h density. We plot together the quasiparticle energies $\xi_{e,k}$ and $\xi_{h,k}$, which clearly shows that our definition is quite reasonable. The spectrum at low e-h density in the first panel [Fig. 4(a)] has not only a well-defined main quasiparticle branch, but also a nearly flat branch with weak intensity, which corresponds to the *exciton-satellite peak*. The fact that both quasiparticle energies and the excitonic satellite are properly reproduced here guarantees the validity of calculation on the ionization ratio we presented above. One finds that the interaction does not affect the mass of dispersion, but that it only influences the band-gap renormalization. This supports the *rigid-band-shift* picture.

With increasing e-h density, both quasiparticle and exciton-satellite branches broaden and start to merge as shown in the second panel [Fig. 4(b)]. The long low-energy tail can be understood as a remnant of the excitonic bound state. In the high-density limit in Fig. 4(c), the spectral broadening is not only further enhanced, but also exhibits the interesting feature mentioned below. In the upper panel, we plot the "shadow" of the hole energy dispersion $\mu - \xi_{h,k}$ in the white line. Then, we can see that the spectral weight of $A_e(k,\omega)$ spreads mainly in the region $\omega > \xi_{e,k}$ and $\omega > \mu - \xi_{h,k}$, or the region $\omega < \xi_{e,k}$ and $\omega < \mu - \xi_{h,k}$. This spectral weight redistribution is understood as the tendency of the mode repulsion at $\omega = \mu_e$ due to the mixing of the "original" dispersion $\xi_{e,k}$ and the "shadow" one $\mu - \xi_{h,k}$ via the e-h interaction or, equivalently, as a precursor behavior of the e-h Cooper pairing.[99] A corresponding feature of $A_h(k,\omega)$ is also found in the lower panel.

Figure 5 shows the single-particle spectra at higher temperature. Again, at low e-h density [Fig. 5(a)], we see the exciton-satellite branch, whereas its dispersion is almost parallel to the main quasiparticle branch and extends towards larger k values. The broadening of both dispersions with increasing n is the same overall with Fig. 4, but this time, the quasiparticle peaks always show large energy tails in both low- and high-energy sides at high e-h density, and the precursor behavior of the e-h Cooper pairing is absent.

We can also evaluate the single-particle spectra in the low e-h density limit by neglecting the trionic (three-body) correlations, which is given as

$$A_a(k,\omega) = 2\pi\left(1 - \sum_{n,q} c_{a,n,q,k}\right)\delta(\omega - \epsilon_{a,k}/\hbar) + 2\pi\sum_{n,q} c_{a,n,q,k}\,\delta(\omega - E_{n,q}/\hbar + \epsilon_{\bar{a},q-k}/\hbar), \tag{51}$$

$$c_{a,n,q,k} = 2|\phi_n[k - (m_a/M)q]|^2[f_B(E_{n,q} - \mu) + f_F(\epsilon_{\bar{a},q-k} - \mu_{\bar{a}})], \tag{52}$$

with $\bar{a} =$ h and e for $a =$ e and h, respectively.[3] The energy of the exciton with momentum q is denoted as $E_{n,q} = E_n + \hbar^2q^2/2M$, where E_n denotes the nth exciton level described by the wave function $\phi_n(k)$ in the momentum space. The first and the second terms correspond to the main quasiparticle and exciton-satellite branches, respectively. At extremely low temperature, as expected, the system behaves as an insulating exciton gas: both the electron and hole single-particle spectra show energy gaps, and their chemical potential lies at around the center of each energy gap, which results in $\mu \sim E_g - E_{1D}$.

The exciton-satellite branch has a negative-mass dispersion $\hbar\omega_{a,k} \sim E_g - E_{1D} - \epsilon_{\bar{a},k}$ since the contribution of $n = 0$ and $q = 0$ is enhanced by the thermal distribution function $f_B(E_{n,q} - \mu)$. At higher temperature, the contribution at $q \neq 0$ can also be important, among which the terms satisfying $n = 0$ and $k - (m_a/M)q \sim 0$ are the most relevant due to the factor of $|\phi_n|^2$. As a result, the dispersion of exciton-satellite branch is approximately given as $\hbar\omega_{a,k} \sim \epsilon_{a,k} - E_{1D}$, which is parallel to the main quasiparticle branch. The gradual change in the mass of the exciton-satellite dispersion from negative to positive values is seen in $A_e(k,\omega)$ shown in the upper panels of Figs. 4(a) and 5(a).

As e-h density is increased at low temperature, the exciton-satellite structure near $k = 0$ is broadened but is almost unshifted in energy located at around $E_g/2 - E_{1D}$ due to the charge neutrality of the e-h pair. This implies that the remnant of the exciton satellite still remains even at around the Mott density: even when the band-gap renormalization becomes comparable to the exciton binding energy $E_g - E_g^* \sim E_{1D}$, the exciton-satellite structure at around $E_g/2 - E_{1D}$ still lies below the effective band edge at around $E_g^*/2$. Therefore, we do not see the complete ionization at the Mott density,[71] whereas the excitonic fraction $1 - \alpha$ is of the order of several percent at most. Here, the effective ionization energy for an electron or a hole in the exciton-satellite states is roughly estimated as $E_g^*/2 - (E_g/2 - E_{1D}) \sim E_{1D}/2$, which also gives the reason why the discontinuity in the e-h chemical potential is close to $E_{1D}/2$ at the pure Mott transition.

D. Interband optical spectra

Now, let us discuss the interband optical spectra. Figure 6 shows the e-h density dependence of absorption-gain spectra for several choices of temperature. The spectra are evaluated in two different ways, one by means of our SSTA and the other by the SBE.

In our SSTA, the intercarrier scattering process gives an intrinsic broadening. By contrast, in SBE calculation, this broadening is absent. Thus, we introduce a phenomenological broadening *by hand* by taking a convolution with the Lorentzian with half-width $\gamma = E_{1D}/14 \sim 1$ meV. This difference can be seen in the n and T dependencies of the linewidth of the excitonic peak located at $\hbar\Omega \sim E_g - E_{1D}$. It is enhanced as n or T increases in our SSTA, but trivially not in SBE.

Another difference appears in the n dependence of the peak energy of the absorption spectra. At low e-h density, our SSTA results exhibit the excitonic peak almost unshifted or slightly blue-shifted, while it is slightly red-shifted in SBE results. As shown in Fig. 6(c), when and only when the temperature and the e-h density are close to the unstable region in the phase diagram, the peak shows a red-shift also in our calculation, which is interpreted as the precursor of thermodynamic instability, and should be distinguished from that seen at higher temperature. The absorption peak starts to show a blue-shift when n exceeds $n_P(T)$. This blue-shift is almost parallel to that of the e-h chemical potential because the excitonic enhancement (Coulomb enhancement) of spectra works at $\hbar\Omega \sim \mu$.

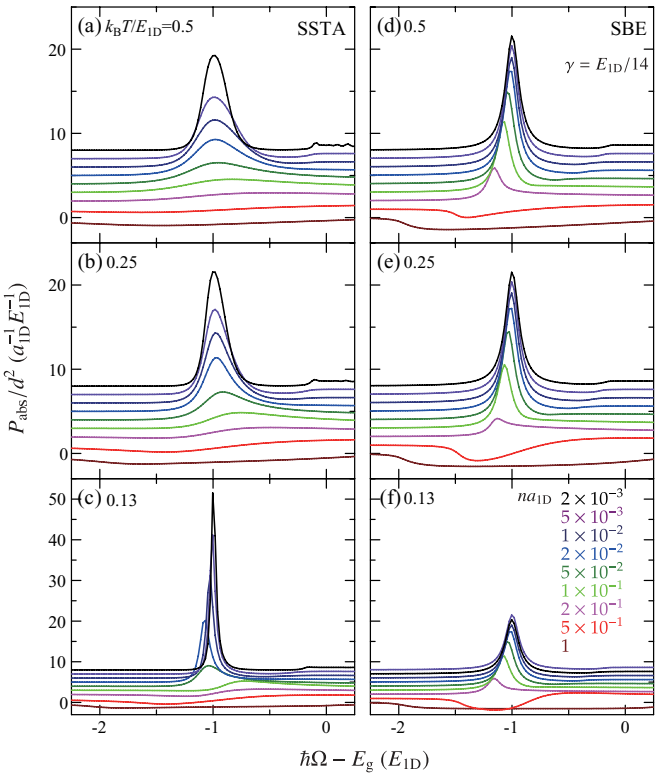

FIG. 6. (Color online) Absorption-gain spectra evaluated with our SSTA at (a) $k_BT/E_{1D} = 0.5$, (b) 0.25, and (c) 0.13. Those calculated using SBE at corresponding temperatures are also shown in (d)–(f) for comparison. Electron-hole density is changed from $na_{1D} = 2 \times 10^{-3}$ to 1.

We can also see the third difference in the band-edge threshold, which is the stepwise structure at the renormalized band gap $\hbar\Omega = E_g^*$. In our SSTA, this threshold can be confirmed in the spectra only at the low e-h density because the spectral broadening smears out this fine structure. At such low-n region, this threshold is almost unshifted, reflecting the strong suppression of BGR. By contrast, SBE results show the red-shift from the extremely low e-h density, and the spectral threshold is clearly seen in the spectra up to around the plasma-gain-onset density $n \lesssim n_P(T)$.

The fourth difference is found in the low-energy spectral tail of the optical gain. Both in our SSTA and in SBE spectra, the optical gain, namely, the negative absorption, does appear and grows up at $n \gtrsim n_P(T)$. Its spectral structure is much more smeared in our SSTA than in the SBE, as most significantly seen in the long tails in the lower-energy side. These low-energy tails are far from those of the Lorentzian function and never reproduced even if we tune the broadening parameter γ in the SBE calculation. The appearance of optical gain contradicts the results of Ref. 39, which predicts the vanishingly small gain, buried in the huge spectral broadening. This contradiction is ascribed to the shortcomings of the Shindo approximation[92] used there.

In Fig. 7(a), the optical-gain spectra $-P_{abs}(\Omega)$ at $k_BT = 0.25E_{1D}$ are examined in detail from the intermediate to the high e-h density. Here, we compare the results with and without vertex corrections in the solid and the broken lines, which we evaluate using $\mathrm{Im}\mathcal{G}_{eh}$ and $\mathrm{Im}\mathcal{G}_{eh}^{(0)}$, including and

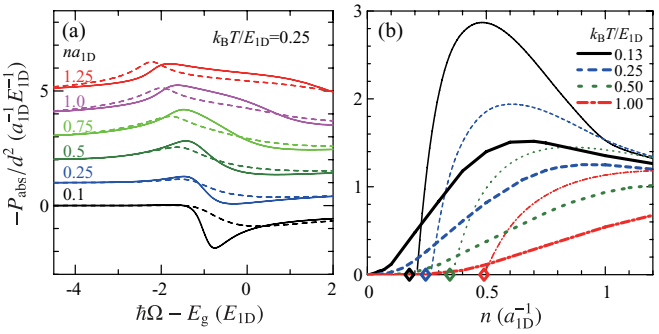

FIG. 7. (Color online) (a) Optical gain spectra at $k_BT/E_{1D} = 0.25$ for several choices of e-h density, na_{1D} =0.1, 0.25, 0.5, 0.75, 1.0, and 1.25. Spectra evaluated with and without vertex corrections are shown in solid and broken lines, respectively. (b) Maximum value of optical-gain spectra as a function of e-h density, which are evaluated with our SSTA (thick lines) and with SBE (thin lines). Results at $k_BT/E_{1D} = 0.13$, 0.25, 0.5, and 1 are shown. Diamond symbols indicate the plasma-gain-onset densities, which are approximated by Eq. (28).

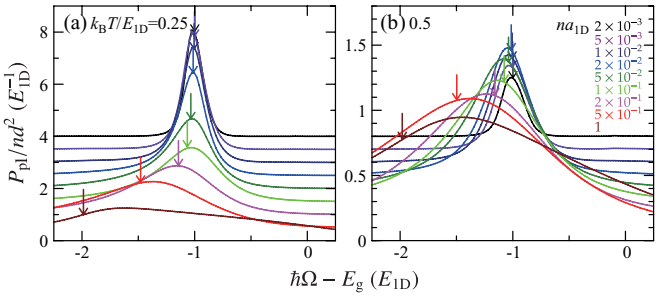

FIG. 8. (Color online) Photoluminescence spectra at (a) $k_BT/E_{1D} = 0.25$, (b) 0.5. Electron-hole density na_{1D} is changed from 2×10^{-3} to 1. Arrows show the ground-state energy of effective Hamiltonian used in SBE, which denotes quasiexciton energy or renormalized band gap, depending on whether e-h density is below or above Mott density.

neglecting the excitonic effects, respectively. One finds that the excitonic correlation enhances the broad structure near $\hbar\Omega \sim \mu$ (excitonic enhancement), and instead the spectral weight at the band edge $\hbar\Omega \sim E_g^*$ is suppressed. This intensity transfer can be understood within the SBE framework, and is discussed elsewhere.[64] In spite of this intensity transfer, the gain peak still stays at slightly above the renormalized band edge, which is the vestige of the divergence in the free-carrier joint density of states. This is the characteristic feature of 1D e-h systems. In 2D and 3D systems, the gain peak locates near the e-h chemical potential μ, where the excitonic enhancement at around $\hbar\Omega \sim \mu$ forms the peak structure.

The *gradual* growth of the optical gain at $n \sim n_P(T)$ can be viewed as a classical-quantum crossover in our SSTA. This makes sharp contrast with the SBE results showing a clear optical-gain threshold at $n = n_P(T)$. In fact, our gain spectra exhibit a so-called *excitonic gain* even at $n < n_P(T)$.[41–46,66–69,72,73] This gain stems from the low-energy tails of the single-particle spectra, which give rise to the finite weight of the joint density of states even at $\hbar\Omega < \mu$.

The difference in the optical-gain growth can be seen more clearly in Fig. 7(b), in which we plot n dependence of the maximum values of the optical gain for several choices of temperature. In both cases, the optical gain becomes relevant near the plasma-gain-onset density given by Eq. (28), as indicated in the diamond symbols. The difference is that the gain increases smoothly from the lowest density in our SSTA, while shows clear thresholds in the SBE.

The maximum value of the optical gain is an increasing function of n at low n, while it turns into a decreasing function at high n. This nonmonotonic n dependence can be seen in both our SSTA and the SBE spectra,[63] whereas the free-carrier theory predicts that the gain maximum increases monotonically. The optical-gain peak near the renormalized band edge is suppressed by the above-mentioned intensity-transfer mechanism in the many-body calculations, while it is absent in the free-carrier theory. In our SSTA, it is further smeared out forming the long low-energy spectral tail. Since the gain suppression near the renormalized band edge is more emphasized at higher e-h density, the maximum value of the optical-gain spectra is decreased.

We finally show the photoluminescence spectra in Fig. 8. In the low-n region $n \lesssim n_P(T)$, the excitonic peak is located at $\hbar\Omega \sim E_g - E_{1D}$, and is slightly red-shifted. It is interesting that the peak of the absorption spectra is almost unshifted or slightly blue-shifted, while that of the PL spectra is slightly red-shifted in our SSTA. This makes sharp contrast with the SBE results, where both the absorption and the PL spectra show red-shifts at $n \lesssim n_P$. In our SSTA, the Moss-Burstein effects, namely, the phase-space-filling effects on the optical spectra, start to work below the plasma-gain-onset density.

The red-shifts of the PL peak start enhanced when n exceeds $n_P(T)$. In this high-n region, the peak positions of the PL and optical-gain spectra are almost similar and locate slightly above the renormalized band gap $\hbar\Omega = E_g^*$, which is a decreasing function of n. Together with this enhancement of the red-shifts, we can also see the rapid spectral broadening. This broadening is attributable to the Moss-Burstein effect. The energy range of the relevant spectral intensity $E_g^* \lesssim \hbar\Omega \lesssim \mu$ becomes wider since E_g^* and μ are the decreasing and increasing functions of n, respectively.

At low temperature $k_BT \lesssim E_{1D}$, the PL peak energy is well reproduced by the ground-state energy of the effective Hamiltonian $\hat{H}_{Q=0}$ used in SBE. Interestingly enough, the quasiexciton energy obtained by SBE formalism is rather close to the PL peak than the excitonic peak in the absorption-gain spectra. This implies that the excitonic peak in the absorption-gain spectra is affected by the Moss-Burstein effects and thus blue-shifted.

Our results on the interband optical spectra are summarized in Fig. 9. We plot the n dependence of the peak energies of the absorption, gain, and PL spectra together with the upper and lower half-widths of the peak. The n dependence of the quasiexciton energy, renormalized band gap, and e-h chemical potential are also shown.

As already discussed above, the most dominant spectral changes are found in the quantum-crossover at around $n \sim n_P$. In fact, the spectral characteristics of the e-h plasma is strongly enhanced at $n \gtrsim n_P$. We can also see another quantum crossover at around $n \sim n_{min} (\ll n_P)$ where the ionization

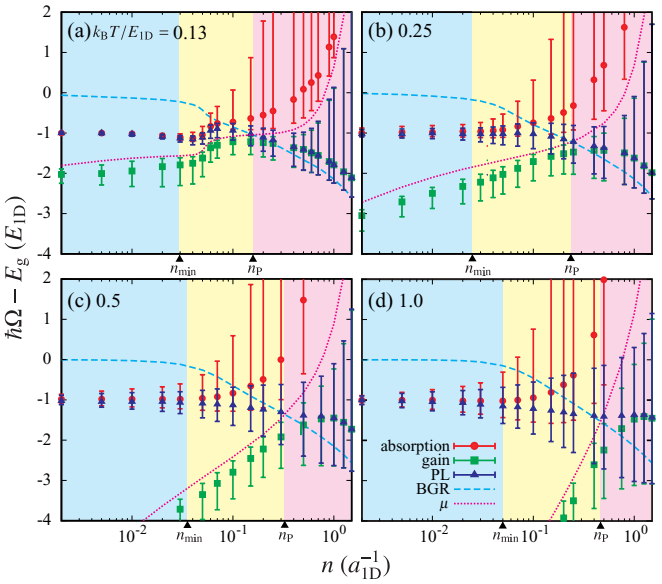

FIG. 9. (Color online) Summary of our results on interband optical spectra at (a) $k_BT/E_{1D} = 0.13$, (b) 0.25, (c) 0.5, and (d) 1.0. Peak energy of the absorption, gain, and photoluminescence spectra are shown by circle, square, and triangle, respectively, together with error bars denoting the upper and lower half-widths of the peak. Renormalized band gap and e-h chemical potential are also shown in broken and dotted lines, respectively. Renormalized band gap, e-h chemical potential, and PL peak energy cross almost simultaneously at around plasma-gain-onset density n_P (shown in the thick broken line in Fig. 2). The e-h density corresponding to the minimum of ionization ratio is denoted by n_{min} (shown in the thick dotted line in Fig. 2).

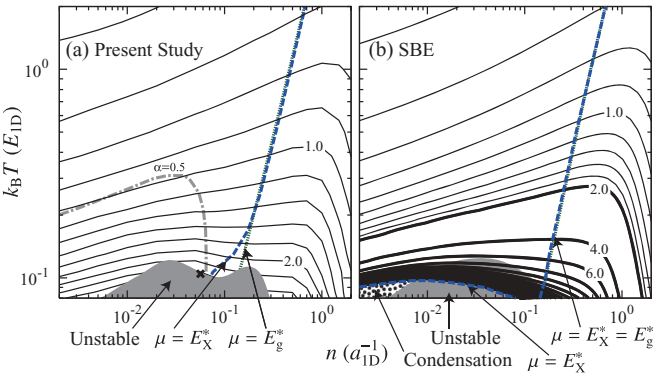

FIG. 10. (Color online) Contour plot of the e-h pair susceptibility evaluated in units of $E_{1D}^{-1}a_{1D}^{-1}$ by (a) our SSTA and (b) SBE. On broken and dotted lines, e-h chemical potential μ coincides with renormalized band gap E_g^* and with SBE quasiexciton energy E_X^*, respectively. The e-h pair susceptibility diverges on the boundary of the hatched region, which appears only in the SBE result. Isothermal compressibility diverges on the boundary of the gray region, inside which a homogeneous thermodynamic state is unstable. Chain line denotes the contour of the ionization ratio $\alpha = 0.5$.

ratio is minimized and the quantum dissociation begins. The Moss-Burstein effects (energy splitting between the absorption and the PL peaks) and the spectral broadenings start to be relevant there. The band-edge threshold in the absorption spectra is thus smeared out.

Noteworthy is that the e-h chemical potential μ, the renormalized band gap E_g^*, and the PL peak energy cross almost simultaneously at around $n = n_P$. This is a characteristic feature of the quasi-1D system, which can be proved rigorously within the SBE framework, as mentioned in Sec. II D.

E. e-h pair susceptibility

The contour plot of the e-h pair susceptibility is given in Figs. 10(a) and 10(b), which are evaluated by our SSTA and the SBE, respectively. We also plot the condition $\mu = E_X^*$, where E_X^* denotes the quasiexciton energy estimated by SBE. In our SSTA, the presence of excitonic bound states below the Mott density is accounted for in the evaluation of μ, whereas SBE estimates μ under the assumption of complete ionization. Further, the intercarrier scatterings bring the imaginary parts to the self-energies in our SSTA, but not in SBE. As for the e-h pair condensation, SBE tells us nothing more than the Bardeen-Cooper-Schrieffer (BCS) mean-field theory, while our SSTA partially accounts for the pair fluctuation effects.

With this in mind, let us compare our SSTA and the SBE results. In our SSTA, the e-h pair susceptibility is enhanced as n is lowered, but does not diverge even at the lowest temperature at which our calculations were done. By contrast, in the SBE result, the contours crowd into a single curve at low T, which indicates the divergence of the pair susceptibility. In particular, our SSTA predicts correctly the absence of the exciton Bose-Einstein condensation (BEC) at low e-h density as one expects in the 1D and 2D systems, while SBE predicts incorrectly a condensation at finite temperature.

Such a difference mainly stems from the n dependence of the e-h chemical potential. At high temperature, the prerequisite for BEC, $\mu = E_X^*$, coincides with the plasma-gain-onset condition $\mu = E_g^*$ in both our SSTA and SBE. This is because the renormalized band gap, the e-h chemical potential, and the quasiexciton energy cross (almost) simultaneously, as mentioned in Secs. II D and III D. However, these conditions $\mu = E_X^*$ and $\mu = E_g^*$ define different lines on the phase diagram at low temperature near or inside the unstable region.[100] In our SSTA, the prerequisite for BEC is never satisfied in the low e-h density region: the line denoting $\mu = E_X^*$ is discontinued inside the unstable region, reflecting the pure Mott transition. By contrast, in SBE, the line of $\mu = E_X^*$ runs into the lowest e-h density region. Clearly, neglecting the excitonic effects in the self-energies gives unreasonably high e-h chemical potentials.

Even in the intermediate or high e-h density region, the e-h pair condensation is not found for any calculated parameters of n and T, whereas SBE still predicts a finite-temperature transition. In our SSTA, the divergence of the e-h pair susceptibility is smeared out by the spectral broadening of the intercarrier scatterings, which is enhanced strongly by the low dimensionality. By contrast, SBE predicts unreasonably high transition temperature again because the intercarrier scatterings are completely neglected.

An extraordinary enhancement of the e-h pair susceptibility is found in our SSTA in the n-T region with low ionization ratio region, namely, $\alpha \lesssim 0.5$. There, the excitonic correlation is enhanced because the small ionization ratio is fed back as

the screening suppression resulting in the stabilization of the excitonic bound states.

IV. DISCUSSION: COMPARISON WITH EXPERIMENTS

In this section, we compare our optical spectra with those measured in the most recent experiments.[47,54–57] The absorption-gain spectra observed on the high-quality quantum wire show the following features. At low n, both the excitonic peak and the band-edge threshold are almost unshifted. As n is increased, the spectral broadening is enhanced and the band-edge threshold is smeared out. When n is further increased, the excitonic peak is blue-shifted, and the optical gain (negative absorption) appears in the low-energy side. Appearance of optical gain shows a crossover behavior: small but finite optical gain is seen from low e-h density. The gain spectra have long low-energy tails, which can not be explained by the broadening of Lorentzian type.

Our theory succeeds in explaining all the above aspects of the experimental observation, as already mentioned in the previous section. It makes sharp contrast to the SBE ones which show artificial red-shifts in the excitonic peak as well as in the band-edge threshold, and do not explain the many-body spectral broadening.

Agreement between our theory and the experiment is quantitative with respect to the spectral peak energies and their intensities. Although the spectral broadening is somewhat overestimated, the detailed spectral shape is qualitatively reproduced. This overestimation is presumably attributable to the oversimplification of the model interaction potential mentioned in Sec. II A, and the overestimation of the multiple intercarrier scattering effects in the self-consistent T-matrix approximation.

As for the PL spectra, our theory is still insufficient since it fails to explain the two-peak structure found in experiments. One possibility is that the low- and high-energy peaks have the excitonic and biexcitonic origins, respectively. Another possibility is that this double-peak structure is a precursor of inhomogeneity or pure Mott transition found in the lowest-temperature region of our phase diagram. It is noteworthy that an inhomogeneous state (biexcitonic crystallization) is also proposed by the bosonization method.[101] Anyway, we should take into account the trionic (three-body) or the biexcitonic (four-body) correlations in order to clarify this point, which is left for our future problem.

V. SUMMARY

We clarified the features of quasi-one-dimensional electron-hole (e-h) systems by applying a self-consistent screened T-matrix approximation we developed recently, which can deal with an e-h pair embedded in the background of the exciton-plasma mixture, characterized by the concept of exciton ionization ratio. It turned out that the exciton-Mott physics as well as the changes in interband optical spectra can be understood as classical-quantum crossovers.

The onset of the quantum dissociation of the exciton (binding-energy reduction and level-broadening effects) defines a classical-quantum crossover at $n\lambda_{\mathrm{T}} \sim 0.2$ in our GaAs quantum wire, where n and λ_{T} are the e-h density and the thermal de Broglie length defined with the e-h reduced mass, respectively. At lower temperature, an inhomogeneous phase with some first-order phase transitions is expected since not only the divergence in the compressibility but also the discontinuous change in the ionization ratio is found.

Another classical-quantum crossover is found in the changes of interband optical spectra. In the low-n region, both the excitonic peak and the band-edge threshold are almost unshifted in energy in the absorption-gain spectra. In the high-n region, enhanced Moss-Burstein effects are seen in the absorption-gain and photoluminescence spectra, and the optical gain does appear with the long low-energy tails caused by the intercarrier scattering. The spectral changes between these two regions take place gradually at $n\lambda_{\mathrm{T}} \sim 1.21 \times (M/m)^{1/4}$, where m and M denote the reduced and the total mass of an e-h pair, respectively.

ACKNOWLEDGMENTS

The authors thank K. Kamide for pointing out the coincidence between the Mott and the plasma-gain-onset densities when the SBE is applied to models with short-range interaction.[102] The authors also thank H. Akiyama and M. Yoshita for discussion. This work is supported by KAKENHI (Grants No. 20104010 and No. 21740231).

APPENDIX: DERIVATION OF EQ. (28)

In this Appendix, we derive Eq. (28). We consider the criterion of the plasma-gain onset

$$\mu - E_{\mathrm{g}^*} = \sum_{a=\mathrm{e,h}} (\mu_a - \xi_{a,k=0}) = 0 \tag{A1}$$

in the D-dimensional e-h systems. Our purpose here is to rewrite this condition in terms of the e-h density n and the temperature T.

As already discussed in Sec. III C, the rigid-band-shift picture works pretty well at high-n region, e.g., near the plasma-gain onset. The quasiparticle energy $\xi_{a,k}$ is well approximated by

$$\xi_{a,k} \sim \frac{\hbar^2 k^2}{2m_a} + \xi_{a,k=0} \tag{A2}$$

with the bare masses of the electron and the hole m_{e} and m_{h}. This implies that the relation among n, T, μ_{e}, and μ_{h} can be evaluated by the free-carrier theory as

$$n\lambda_{\mathrm{T}}^D \left(\frac{m}{m_a}\right)^{D/2} = 2I_{D/2-1}\left(\frac{\mu_a - \xi_{a,k=0}}{T}\right) \tag{A3}$$

in D-dimensional e-h system, where

$$I_\nu(x) = \frac{1}{\Gamma(\nu+1)} \int_0^\infty \frac{\epsilon^\nu}{\exp(\epsilon - x) + 1} d\epsilon \tag{A4}$$

denotes the complete Fermi-Dirac integral of order ν. Let us rewrite Eq. (A3) to

$$n\lambda_{\mathrm{T}}^D \left(\frac{m}{M}\right)^{D/4} = 2[I_{D/2-1}(x_{\mathrm{e}}) I_{D/2-1}(x_{\mathrm{h}})]^{1/2}, \tag{A5}$$

$$I_{D/2-1}(x_{\mathrm{e}}) = \left(\frac{m_{\mathrm{h}}}{m_{\mathrm{e}}}\right)^{D/2} I_{D/2-1}(x_{\mathrm{h}}), \tag{A6}$$

with $x_a = (\mu_a - \xi_{a,k=0})/T$. In principle, the right-hand side of Eq. (A5) can be rewritten as a function of $x = x_e + x_h$ and $\delta = (m_e - m_h)/(m_e + m_h)$ by using Eq. (A6). It is independent of δ in the classical limit $e^x \ll 1$:

$$2[I_{D/2-1}(x_e)I_{D/2-1}(x_h)]^{1/2} \sim \text{const} \times e^x. \tag{A7}$$

The δ dependence is still weak for small $|\delta|$ even in the semiquantum regime $e^x \sim 1$ because the right-hand side of Eq. (A5) is an even function of δ and its derivative vanishes at $\delta = 0$. (In our model, the value of δ is about 0.25.) Thus, it is reasonable to estimate the right-hand side of Eq. (A5) by setting $\delta = 0$.

Then, we can write the criterion of the plasma-gain onset, $x = 0$, as

$$n\lambda_T^D = 2\left(\frac{M}{m}\right)^{D/4} I_{D/2-1}(0) \tag{A8}$$

in terms of n and T since Eq. (A6) immediately gives $x_e = x_h = 0$ for $x = 0$ and $\delta = 0$. The complete Fermi-Dirac integral is computed numerically as

$$I_{D/2-1}(0) = \begin{cases} 0.604899 & (D = 1), \\ \ln 2 = 0.693147 & (D = 2), \\ 0.765147 & (D = 3). \end{cases} \tag{A9}$$

The validity of the above approximation can be confirmed by comparing the solid and the broken lines in Fig. 2.

[1] N. F. Mott, Philos. Mag. **6**, 287 (1961).
[2] R. Zimmermann, K. Kilimann, W. D. Kraeft, D. Kremp, and G. Röpke, Phys. Status Solidi B **90**, 175 (1978).
[3] R. Zimmermann, *Many-Particle Theory of Highly Excited Semiconductors* (BSB Teubner, Leipzig, 1987).
[4] S. Schmitt-Rink, J. Löwenau, and H. Haug, Z. Phys. B **47**, 13 (1982).
[5] J. P. Löwenau, S. Schmitt-Rink, and H. Haug, Phys. Rev. Lett. **49**, 1511 (1982).
[6] H. Haug and S. Schmitt-Rink, Prog. Quantum Electron. **9**, 3 (1984).
[7] M. Lindberg and S. W. Koch, Phys. Rev. B **38**, 3342 (1988).
[8] H. Haug and S. W. Koch, *Quantum Theory of the Optical and Electronic Properties of Semiconductors* (World Scientific, Singapore, 2009).
[9] W.-D. Kraeft, D. Kremp, W. Ebeling, and G. Röpke, *Quantum Statistics of Charged Particle Systems* (Plenum, Berlin, 1986).
[10] D. Kremp, M. Schlanges, and W.-D. Kraeft, *Quantum Statistics of Nonideal Plasmas* (Springer, Berlin, 2005).
[11] L. V. Keldish, in *Proceedings of the 9th International Conference on the Physics of Semiconductors* (Nauka, Leningrad, 1968), p. 1303.
[12] M. Combescot and P. Nozières, J. Phys. C: Solid State Phys. **5**, 2369 (1972).
[13] W. F. Brinkmann and T. M. Rice, Phys. Rev. B **7**, 1508 (1973).
[14] T. M. Rice, in *Solid State Physics*, Vol. 32, edited by H. Ehrenreich, F. Seitz, and D. Turnbull (Academic, New York, 1977).
[15] P. Vashishta, P. Bhattacharyya, and K. S. Singwi, Phys. Rev. B **10**, 5108 (1974); **10**, 5127 (1974).
[16] R. N. Silver, Phys. Rev. B **8**, 2403 (1973).
[17] G. Mahler, Phys. Rev. B **11**, 4050 (1975).
[18] H. Haug, Z. Phys. B **24**, 351 (1976).
[19] D. W. Snoke and J. D. Crawford, Phys. Rev. E **52**, 5796 (1995).
[20] L. V. Keldish and A. N. Kozlov, Zh. Eksp. Teor. Pis'ma **5**, 238 (1967) [JETP Lett. **5**, 190 (1967)].
[21] L. V. Keldish and A. N. Kozlov, Zh. Eksp. Teor. Fiz. **54**, 978 (1968) [Sov. Phys.–JETP **27**, 521 (1968)].
[22] E. Hanamura, J. Phys. Soc. Jpn. **29**, 50 (1970); **37**, 1545 (1974).
[23] S. A. Moskalenko and D. Snoke, *Bose-Einstein Condensation of Excitons and Biexcitons* (Cambridge University Press, New York, 2000).
[24] J. des Cloizeaux, J. Phys. Chem. Solids **26**, 259 (1965).
[25] L. V. Keldish and Yu. V. Kopaev, Fiz. Tverd. Tela **6**, 2791 (1964) [Sov. Phys. Solid State **6**, 2219 (1965)].
[26] R. Zimmermann, Phys. Status Solidi B **76**, 191 (1976).
[27] A. P. Silin, Fiz. Tverd. Tela **19**, 134 (1977) [Sov. Phys. Solid State **19**, 77 (1977)].
[28] A. J. Leggett, J. Phys. Colloq. C **7**, 19 (1980).
[29] C. Comte and P. Nozières, J. Phys. (Paris) **43**, 1069 (1982); **43**, 1083 (1982).
[30] P. Nozières and S. Schmitt-Rink, Low. Temp. Phys. **59**, 195 (1985).
[31] For the diversity of Mott physics, see, for example, *Metal-to-Nonmetal Transitions*, edited by R. Redmer, B. Holst and F. Hensel (Springer, Berlin, 2010).
[32] N. Holonyak, Jr., R. M. Kolbas, R. D. Dupuis, and P. D. Dapkus IEEE J. Quantum Electron. **QE-16**, 170 (1980).
[33] Y. Arakawa and H. Sakaki, Appl. Phys. Lett. **40**, 939 (1982).
[34] M. Asada, Y. Miyamoto, and Y. Suematsu, Jpn. J. Appl. Phys. **24**, L95 (1985).
[35] E. Kapon, in *Quantum Well Lasers*, edited by P. S. Zory (Academic, San Diego, 1993).
[36] R. Loudon, Am. J. Phys. **27**, 649 (1959).
[37] T. Ogawa and T. Takagahara, Phys. Rev. B **43**, 14325 (1991); **44**, 8138 (1991).
[38] F. Rossi and E. Molinari, Phys. Rev. Lett. **76**, 3642 (1996); Phys. Rev. B **53**, 16462 (1996).
[39] D. W. Wang and S. Das Sarma, Phys. Rev. B **64**, 195313 (2001).
[40] E. Kapon, D. M. Hwang, and R. Bhat, Phys. Rev. Lett. **63**, 430 (1989).
[41] W. Wegscheider, L. N. Pfeiffer, M. M. Dignam, A. Pinczuk, K. W. West, S. L. McCall, and R. Hull, Phys. Rev. Lett. **71**, 4071 (1993).
[42] W. Wegscheider, L. Pfeiffer, M. Dignam, A. Pinczuk, K. West, and R. Hull, Semicond. Sci. Technol. **9**, 1933 (1994).
[43] S. Tiwari, G. D. Pettit, K. R. Mikove, F. Legous, R. J. Favis, and J. M. Woodall, Appl. Phys. Lett. **64**, 3536 (1994).
[44] L. Sirigu, D. Y. Oberli, L. Degiorgi, A. Rudra, and E. Kapon, Phys. Rev. B **61**, 10575 (2000).
[45] L. Sirigu, L. Degiorgi, D. Y. Oberli, A. Rudra, and E. Kapon, Phys. E (Amsterdam) **7**, 513 (2000).
[46] J. Rubio, L. Pfeiffer, M. H. Szymanska, A. Pinczuk, S. He, H. U. Baranger, P. B. Littlewood, K. W. West, and B. S. Dennis, Solid State Commun. **120**, 423 (2001).

[47]Y. Hayamizu, M. Yoshita, S. Watanabe, H. Akiyama, L. N. Pfeiffer, and K. W. West, Appl. Phys. Lett. **81**, 4937 (2002).
[48]H. Akiyama, L. N. Pfeiffer, M. Yoshita, A. Pinczuk, P. B. Littlewood, K. W. West, M. J. Matthews, and J. Wynn, Phys. Rev. B **67**, 041302 (2003).
[49]R. Cingolani, H. Lage, L. Tapfer, H. Kalt, D. Heitmann, and K. Ploog, Phys. Rev. Lett. **67**, 891 (1991).
[50]R. Cingolani, R. Rinaldi, M. Ferrara, G. C. La Rocca, H. Lage, D. Heitmann, K. Ploog, and H. Kalt, Phys. Rev. B **48**, 14331 (1993).
[51]Ch. Gréus, A. Forchel, R. Spiegel, F. Faller, S. Benner, and H. Haug, Europhys. Lett. **34**, 213 (1996).
[52]R. Ambigapathy, I. Bar-Joseph, D. Y. Oberli, S. Haacke, M. J. Brasil, F. Reinhardt, E. Kapon, and B. Deveaud, Phys. Rev. Lett. **78**, 3579 (1997).
[53]T. Guillet, R. Grousson, V. Voliotis, M. Menant, X. L. Wang, and M. Ogura, Phys. Rev. B **67**, 235324 (2003).
[54]Y. Hayamizu, M. Yoshita, Y. Takahashi, H. Akiyama, C. Z. Ning, L. N. Pfeiffer, and K. W. West, Phys. Rev. Lett. **99**, 167403 (2007).
[55]M. Yoshita, S.-M. Liu, M. Okano, Y. Hayamizu, H. Akiyama, L. N. Pfeiffer, and K. W. West, J. Phys.: Condens. Matter **19**, 295217 (2007).
[56]M. Yoshita, M. Okano, T. Ihara, H. Akiyama, P. Huai, T. Ogawa, L. N. Pfeiffer, and K. W. West, Phys. Status Solidi C **5**, 2841 (2008).
[57]H. Akiyama, M. Yoshita, Y. Hayamizu, S.-M. Liu, M. Okano, L. N. Pfeiffer, K. W. West, K. Asano, T. Ogawa, and C. Z. Ning, Phys. E (Amsterdam) **40**, 1726 (2008).
[58]T. Ihara, S. Maruyama, M. Yoshita, H. Akiyama, L. N. Pfeiffer, and K. W. West, Phys. Rev. B **80**, 033307 (2009).
[59]H. Akiyama (private communication).
[60]B. Tanater, J. Phys.: Condens. Matter **8**, 5997 (1996).
[61]E. H. Hwang and S. Das Sarma, Phys. Rev. B **58**, R1738 (1998).
[62]S. Benner and H. Haug, Europhys. Lett. **16**, 579 (1991).
[63]P. Huai, H. Akiyama, Y. Tomio, and T. Ogawa, Jpn. J. Appl. Phys. **46**, L1071 (2007).
[64]M. Okano, P. Huai, M. Yoshita, S. Inada, H. Akiyama, K. Kamide, K. Asano, and T. Ogawa, J. Phys. Soc. Jpn. **80**, 114716 (2011).
[65]S. Das Sarma and D. W. Wang, Phys. Rev. Lett **84**, 2010 (2000).
[66]C. Piermarocchi, V. Savona, A. Quattropani, P. E. Selvmann, P. Schwendimann, and F. Tassone, Phys. Status Solidi B **206**, 455 (1998).
[67]F. Tassone and C. Piermarocchi, Phys. Rev. Lett. **82**, 843 (1999).
[68]C. Piermarocchi, F. Tassone, C. Ciuti, V. Savona, P. Schwendimann, and A. Quattropani, Phys. Status Solidi A **178**, 435 (2000).
[69]C. Piermarocchi and F. Tassone, Phys. Rev. B **63**, 245308 (2001).
[70]T. Hanamiya, K. Asano, and T. Ogawa, Phys. E (Amsterdam) **40**, 1401 (2008).
[71]The exciton ionization ratio is observable by means of terahertz spectroscopy. See, for example, T. Suzuki and R. Shimano, Phys. Rev. Lett. **109**, 046402 (2012). They report that $1s$-$2p$ resonance of the exciton is broadened but remains even above the Mott density in the bulk Si.
[72]R. Schepe, T. Schmielau, D. Tamme, and K. Henneberger, Phys. Status Solidi B **206**, 273 (1998).
[73]T. Schmielau, G. Manzke, D. Tamme, and K. Henneberger, Phys. Status Solidi B **221**, 215 (2000).
[74]Q. Y. Peng, T. Schmielau, G. Manzke, and K. Henneberger, J. Cryst. Growth **214-215**, 810 (2000).
[75]H. Stolz and R. Zimmermann, Phys. Status Solidi B **94**, 135 (1979).
[76]R. Zimmermann and H. Stolz, Phys. Status Solidi B **131**, 151 (1985).
[77]N. H. Kwong, G. Rupper, and R. Binder, Phys. Rev. B **79**, 155205 (2009).
[78]F. X. Bronold and H. Fehske, Phys. Rev. B **74**, 165107 (2006).
[79]D. Semkat, F. Richter, D. Kremp, G. Manzke, W.-D. Kraeft, and K. Henneberger, Phys. Rev. B **80**, 155201 (2009).
[80]F. Richter, D. Semkat, D. Kremp, and K. Henneberger, Phys. Status Solidi C **6**, 532 (2009).
[81]D. Semkat, D. Kremp, and K. Henneberger, Phys. Status Solidi C **6**, 546 (2009).
[82]D. Semkat, F. Richter, D. Kremp, G. Manzke, W.-D. Kraeft, and K. Henneberger, J. Phys.: Conf. Ser. **210**, 012005 (2010).
[83]G. Manzke, D. Semkat, F. Richter, D. Kremp, and K. Henneberger, J. Phys.: Conf. Ser. **210**, 012020 (2010).
[84]T. Yoshioka and K. Asano, Phys. Rev. Lett. **107**, 256403 (2011).
[85]W. Hoyer, M. Kira, and S. W. Koch, Phys. Status Solidi B **234**, 195 (2002).
[86]S. W. Koch, W. Hoyer, M. Kira, and V. S. Filinov, Phys. Status Solidi B **238**, 404 (2003).
[87]V. S. Filinov, H. Fehske, M. Bonitz, V. E. Fortov, and P. Levashov, Phys. Rev. E **75**, 036401 (2007).
[88]In Refs. 85–87, the ionization ratio is evaluated from the e-h pair distribution function: the electron accumulation around a hole (or vice versa) is interpreted as the exciton formation.
[89]See, for example, J. C. Hensel, T. G. Phillips, and G. A. Thomas, in *Solid State Physics*, Vol. 32, edited by H. Ehrenreich, F. Seitz, and D. Turnbull (Academic, New York, 1977).
[90]H. Kalt, R. Nötzel, K. Ploog, and H. Giessen, Phys. Status Solidi B **173**, 389 (1992).
[91]M. Stern, V. Garmider, V. Umansky, and I. Bar-Joseph, Phys. Rev. Lett. **100**, 256402 (2008).
[92]K. Shindo, J. Phys. Soc. Jpn. **29**, 278 (1970).
[93]The Bose distribution functions in Eqs. (23) and (24) do not lead to the divergence of the integrands. In fact, $f_{\rm B}(\Omega){\rm Im}\mathcal{G}^{(0)}_{ab}(k;Q,\Omega)$ does not diverge at $\Omega=0$, as can be seen in Eq. (19). Further, $f_{\rm B}(\Omega){\rm Im}\mathcal{T}_{ab}(k,k';Q,\Omega)$ shows no singularity at $\Omega=0$ since it can be expressed in terms of ${\rm Re}\mathcal{G}^{(0)}_{\rm ab}(k;Q,\Omega)$, $f_{\rm B}(\Omega){\rm Im}\mathcal{G}^{(0)}_{ab}(k;Q,\Omega)$, and ${\rm Re}\mathcal{T}^{(0)}_{ab}(k,k';Q,\Omega)$ by means of Eq. (16). Using Eq. (26), we can also confirm the absence of the divergence of $f_{\rm B}(\Omega){\rm Im}\mathcal{G}_{\rm eh}(k,k';Q,\Omega)$ at $\Omega=0$. Therefore, $P_{\rm abs}(\Omega)$ evaluated by our SSTA should change its sign at $\Omega=\mu$, and $P_{\rm pl}(\Omega)=f_{\rm B}(\Omega-\mu)P_{\rm abs}(\Omega)$ has no trivial divergence there.
[94]D. J. Thouless, Ann. Phys. (NY) **10**, 553 (1960).
[95]R. F. Bishop, M. R. Strayer, and J. M. Irvine, Phys. Rev. A **10**, 2423 (1974).
[96]R. F. Bishop, H. B. Ghassib, and M. R. Strayer, Phys. Rev. A **13**, 1570 (1976).
[97]L. D. Landau and E. M. Lifshitz, *Quantum Mechanics (Non-relativistic Theory)*, 3rd ed. (Butterworth-Heinemann, Oxford, 1958), Sec. 45, Problems 1 and 2.
[98]M. Combescot, Phys. Status Solidi B **86**, 349 (1978).
[99]This phenomenon is understood as the beginning of the pseudogap formation, which is also studied intensively in the high-T_c super-

conductivity and the ultra-cold-atom systems. See, for example, Y. Yanase, T. Jujo, T. Nomura, H. Ikeda, T. Hotta, and K. Yamada, Phys. Rep. **387**, 1 (2003).

[100]Remind that our proof of the equality $n_{\mathrm{M}}(T) = n_{\mathrm{P}}(T)$ is based on the SBE framework, and assumes that the phase transitions do not take place at the temperature T.

[101]K. Asano and T. Ogawa, J. Lumin. **112**, 200 (2005).

[102]This argument only shows the inequality $n_{\mathrm{M}}(T) \leqslant n_{\mathrm{P}}(T)$ if it is directly applied to the realistic e-h system with long-range Coulomb interaction. This is because the screening effect might break the excitons at $n < n_{\mathrm{P}}(T)$, as expected in the three-dimensional e-h systems. Our discussion in Sec. II D shows that the low dimensionality plays an essential role in the proof of the equality $n_{\mathrm{M}}(T) = n_{\mathrm{P}}(T)$.